Check for updates

Self-supporting metal–organic framework-based hydrogen and oxygen electrocatalysts

Xinran Sun,[a] Sibo Wang, [ID] [a] Yidong Hou, [ID] [a] Xue Feng Lu, [ID] *[a] Jiujun Zhang [ID] [b] and Xinchen Wang [ID] *[a]

Towards green production and efficient utilization of hydrogen, developing renewable clean energy technologies based on hydrogen and oxygen electrocatalysis, especially water electrolysis, zinc–air batteries, and fuel cells, is of vital significance. To promote their energy conversion efficiency, low-cost and high-efficiency electrocatalysts are highly desired to accelerate the sluggish kinetics of hydrogen and oxygen electrocatalytic reactions. The emergence of metal–organic frameworks (MOFs) provides new opportunities to obtain high-performance hydrogen and oxygen electrocatalysts with desired composition and structures. However, most of these MOF-based electrocatalysts are powders, resulting in limited active sites, blocked mass/charge transport, and insufficient stability. In this context, we present an up-to-date investigation of self-supporting MOF-based hydrogen and oxygen electrocatalysts with a focus on the synthesis strategy and application. Finally, some personal insights into the current challenges and potential solutions are presented, aiming at providing some guidance for the design and synthesis of advanced self-supporting MOF-based materials in hydrogen/oxygen-related energy technologies.

[a]State Key Laboratory of Photocatalysis on Energy and Environment, College of Chemistry, Fuzhou University, Fuzhou 350108, China. E-mail: luxf@fzu.edu.cn; xcwang@fzu.edu.cn

[b]College of Materials Science and Engineering, Institute of New Energy Materials and Engineering, Fuzhou University, Fuzhou 350108, China

Xinran Sun received her B.Sc. in 2019 from Qilu Normal University and M.Sc. in 2022 from Linyi University. Now, she is a Ph.D. candidate under the supervision of Prof. Xue Feng Lu and Prof. Xianzhi Fu at Fuzhou University. Her current research interest focuses on the design and synthesis of metal–organic frameworks for efficient hydrogen and oxygen electrocatalysts.

Dr Xue Feng Lu is currently a full professor at the State Key Laboratory of Photocatalysis on Energy and Environment, Fuzhou University, China. He obtained his Ph.D. degree in physical chemistry from Sun Yat-sen University in 2017. Subsequently, Dr Lu carried out his postdoctoral research as a research fellow at Nanyang Technological University, Singapore, and a research associate at The Hong Kong Polytechnic University. After finishing his five-year postdoctoral training, he joined Fuzhou University in July 2022. His research interests focus on the design and synthesis of functional micro/nanomaterials for supercapacitors, water electrolysis, fuel cells, and Zn–air batteries. He has published over 50 peer-reviewed papers with more than 10 000 citations (h-index 44) and was selected as the World's Top 2% Scientists identified by Stanford University in 2020–2022 and the Highly Cited Researcher by Clarivate in 2021 and 2022.

This journal is © The Royal Society of Chemistry 2023

J. Mater. Chem. A, 2023, **11**, 13089–13106 | **13089**

1. Introduction

The aggravating energy crisis and environmental pollution initiated by the consumption of limited fossil fuels are incredibly detrimental to the sustainable development of society.[1–3] A compelling vision is the development of renewable clean energy technologies as alternatives to fossil fuels, such as overall water splitting (OWS), zinc–air batteries (ZABs), and fuel cells (FCs).[4–6] As illustrated in Fig. 1, to improve the energy conversion efficiency of OWS, ZABs, and FCs, developing high-performance hydrogen and oxygen electrocatalysts to accelerate the sluggish kinetics of the hydrogen evolution reaction (HER), hydrogen oxidation reaction (HOR), oxygen evolution reaction (OER), and oxygen reduction reaction (ORR) is highly desired.[7–9] Currently, Pt-based metals are recognized as state-of-the-art catalysts for the HER, HOR, and ORR, while Ir- and Ru-based oxides show a favorable performance for the OER.[10–14] However, the scarcity, high price, and inferior durability of these noble metals hinder their widespread applications in the above electrochemical redox reactions.[15,16] Therefore, it is urgent to develop effective strategies to improve the utilization and stability of precious metal electrocatalysts. In addition, transition metal-based catalysts (transition metal alloys, oxides, sulfides, phosphides, hydroxides, etc.) and carbon-based catalysts have attracted extensive attention in recent years.[17–21] However, due to limited active sites, poor intrinsic activity and stability, and slow mass transfer, their electrocatalytic performance needs to be further improved.

Metal–organic frameworks (MOFs), as a class of coordination compounds with high crystallinity and long-range order, are interconnected by the coordination of metal ions/clusters and organic ligands.[7] The periodic structure of MOFs provides active sites that are uniformly dispersed throughout the porous framework, which is a typical feature of homogeneous catalysts, while the nano/microscale solid nature makes MOFs promising heterogeneous catalysts.[22] When MOFs act as carriers or reaction chambers and precious metals act as active sites, the utilization rate and stability of precious metals can be improved. In addition, benefiting from abundant active sites, fast mass transfer, tunable and abundant pores, and well-defined metal nodes/organic ligands, MOFs stand out among non-precious metal electrocatalysts. However, their poor chemical stability and insufficient electrical conductivity limit their wide application in the field of electrocatalysis. To overcome these shortcomings, through direct carbonization or indirect post-treatments, the researchers converted MOFs into functional inorganic materials, namely MOF derivatives. With various compositions (carbon, metal/carbon, metal compound/carbon, metal compounds, etc.) and structures (hollow, porous, framework, hierarchical, yolk–shell, etc.), MOF derivatives usually exhibit enhanced electrical conductivity, robust chemical stability, and high surface area. However, most MOF-based electrocatalysts are reported in powder form, requiring the aid of polymer binders and conductive additives for practical energy devices, which inevitably lead to uneven catalyst distribution and poor charge/mass transport inside the electrode (Fig. 2a).[23–25] Fortunately, self-supporting electrodes, in which electrocatalysts are grown directly on the surface of the current collector (Fig. 2b), have attracted considerable attention as they are characterized by the following advantages. Firstly, the *in situ* growth of catalysts avoids using polymer binders and conductive additives, which can efficiently promote the exposure of active sites and simplify electrode processing.[26] Secondly, the close contact between catalysts and current collectors can not only effectively promote the transfer of electrons between the two but also prevent the agglomeration or shedding of the catalyst.[27,28] Thirdly, the gap between the catalysts can provide rich solid–liquid–gas three-phase reaction interfaces to facilitate mass transfer, especially at high current densities.[29,30] Regarding these fantastic qualities, self-supporting MOF-based electrocatalysts hold great potential in practical energy technologies and thus deserve attention.

Dr Jiujun Zhang is a Professor at Fuzhou University, Adjunct Professor at the University of British Columbia (UBC) and the University of Waterloo, and former Principal Research Officer at the National Research Council of Canada. Dr Zhang received his BS and MSc in electrochemistry from Peking University in 1982 and 1985, and his PhD in electrochemistry from Wuhan University in 1988. He then carried out three terms of postdoctoral research at the California Institute of Technology, York University, and UBC. Dr Zhang has over 30 years of scientific research experience, particularly in the area of electrochemical energy storage and conversion.

Dr Xinchen Wang obtained his B.Sc. and M.Sc. from Fuzhou University and his Ph.D. from The Chinese University of Hong Kong. He was a JSPS postdoctoral researcher at the University of Tokyo and an Alexander von Humboldt fellow at the Max Planck Institute of Colloids and Interfaces in Germany. He was appointed as a professor at Fuzhou University in 2005. He is currently Vice President of Fuzhou University and the Director of the State Key Laboratory of Photocatalysis on Energy and Environment. His research interests cover all aspects of photocatalysis and materials science, especially polymeric carbon nitrides for photocatalysis.

13090 | *J. Mater. Chem. A*, 2023, **11**, 13089–13106

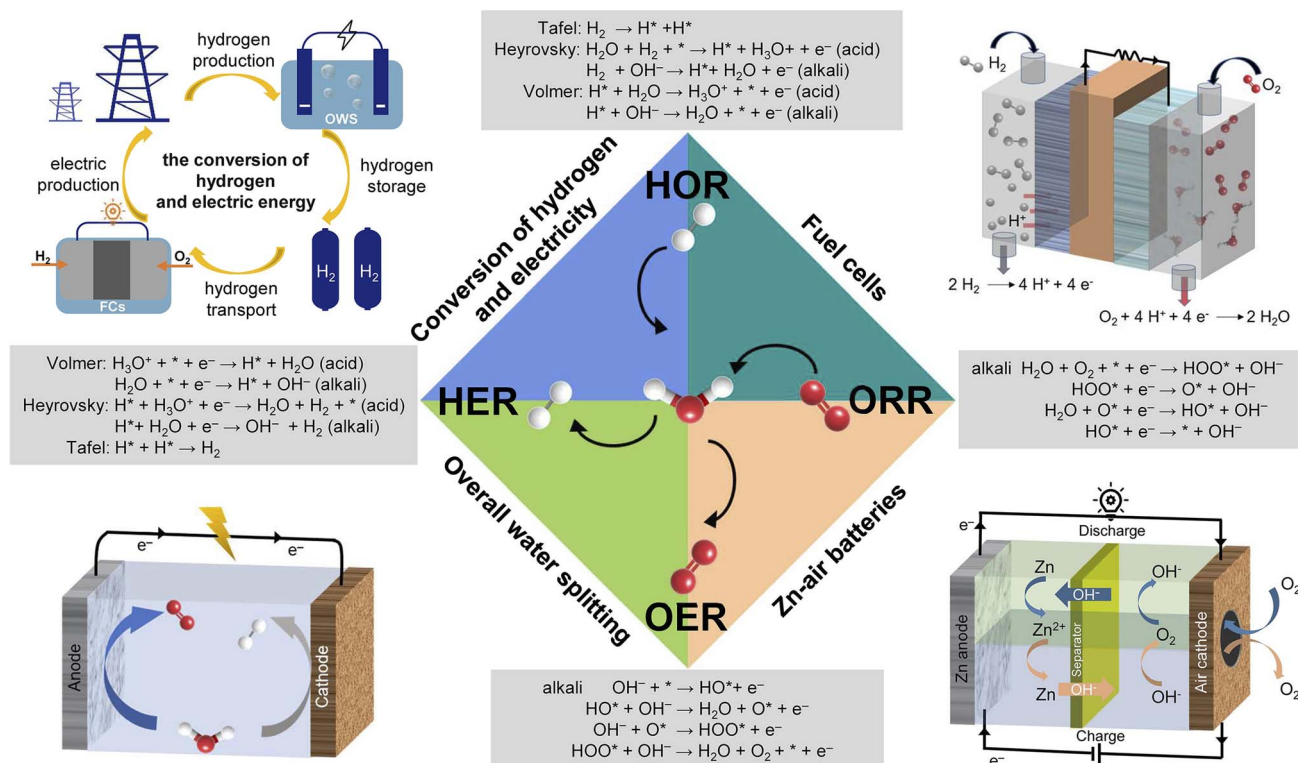This journal is © The Royal Society of Chemistry 2023

Fig. 1 A green cycle between hydrogen and electricity, hydrogen electrocatalyst reaction type and mechanism under acidic/alkaline conditions (* represents the catalytic active site), oxygen electrocatalyst reaction type and mechanism under alkaline conditions, and schematic illustrations of OWS, ZABs, and FCs.

In recent years, many excellent reviews on MOF-based electrocatalysts have been published. However, these reviews focus on a certain type of MOF-based electrocatalyst (i.e., pristine MOFs, MOF compositions, and their derivatives) or a certain catalytic reaction (i.e., the HER, OER, and ORR) and energy conversion technology (i.e., OWS, ZABs, and FCs), and the content mostly revolves around MOF-based powdery electrocatalysts.[22,31–39] Reviews on self-supporting MOF-based electrocatalysts are rarely reported. Recently, Wei et al. gave a critical review of the structural characteristics and fabrication techniques of freestanding MOF-based electrodes for electrochemical energy storage and conversion devices.[24] Li et al. presented the latest research progress in developing MOF-based nanoarrays for electrocatalysis.[40] However, these two reviews about self-supporting MOF-based materials involve too many applications, one from energy storage devices to conversion devices and the other covers almost all catalytic reactions (except the HOR). An up-to-date review of self-supporting MOF-based hydrogen–oxygen electrocatalysts has not been reported. Regarding this, we herein highlight the latest advances focusing on the synthesis strategies of self-supporting MOF-based electrocatalysts and their applications in four types of specific hydrogen/oxygen electrocatalytic reactions, as well as three types of energy devices based on these reactions. Finally, the review concludes with some personal insights into the current challenges and potential solutions, aiming to provide some guidance for advancing self-supporting MOF-based materials in hydrogen/oxygen-related energy technologies.

2. Synthesis strategies

An updated perspective on existing synthetic strategies has far-reaching significance, which points out universal general methods for specific catalysts, stimulates the exploration of emerging strategies, and provides a theoretical basis for the design and synthesis of catalysts. For example, by summarizing synthesis strategies of self-supporting transition metal-based electrodes, Sun et al. pointed out the future application prospects of self-supporting electrocatalysts in the HER and OER.[26] By summarizing the controllable derivation strategies of MOFs into hollow structure materials, Cai et al. provided valuable guidance and inspiration for the preparation of advanced electrocatalysts with ideal structures and compositions.[41] Here, we will summarize the synthesis strategies of self-supporting structures into two categories: pristine MOFs and MOF derivatives.

2.1 Synthesis strategies of self-supporting MOFs

The prerequisite for pristine MOFs to exhibit excellent catalytic performance under harsh electrochemical conditions is to overcome poor electrical conductivity and chemical stability.[42] Recently, active site microenvironment engineering has shown advantages in regulating the physicochemical properties of pristine MOFs.[43] Apart from grafting active catalytic ingredients into MOFs as linkers,[44] many strategies (i.e., defect engineering,[45] ultrathin engineerings,[46] and interface engineering[47])

This journal is © The Royal Society of Chemistry 2023
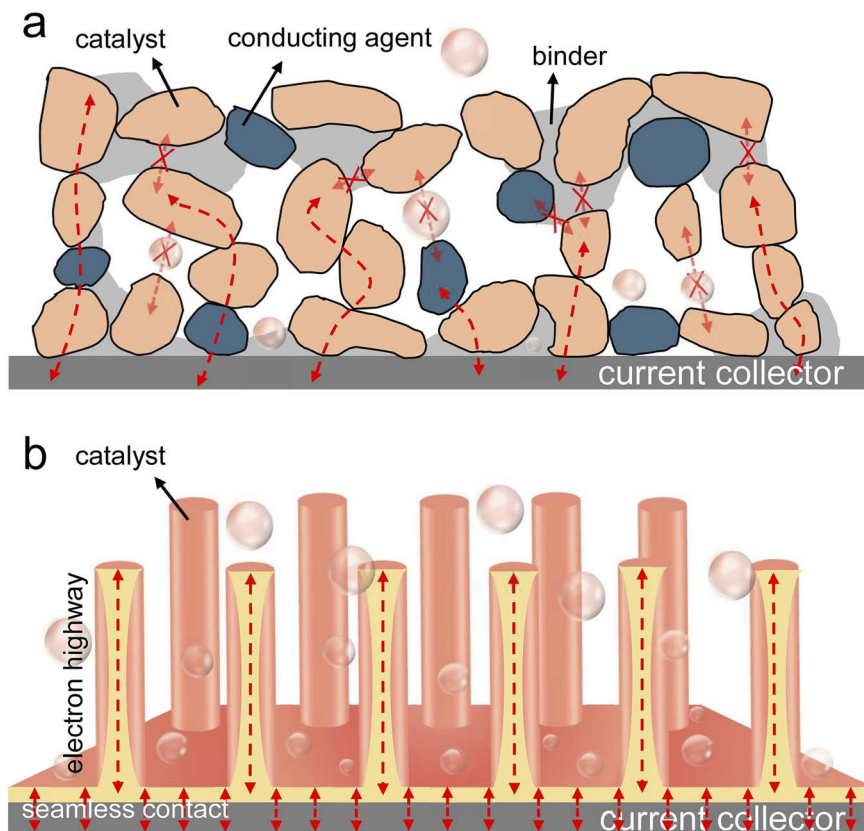
J. Mater. Chem. A, 2023, 11, 13089–13106 | 13091

Fig. 2 Schematic of the internal structure of (a) powdery electrode, in which electrocatalysts are coated on the current collector with the aid of a polymer binder and conductive additives, and (b) self-supporting electrode, in which electrocatalysts are grown directly on the current collector.

have been reported to design advanced electrocatalysts. In addition, a self-supporting structure can also effectively shorten the mass/electron transport distance, thereby improving the conductivity of MOFs and delaying the collapse of the structure.[48,49] Around these two points, we will focus on the latest progress of active site microenvironment engineering in preparing self-supporting pristine MOFs in this section.

2.1.1 One-step synthesis. The hydro/solvothermal method is one of the most common preparation methods for self-supporting MOFs with high crystallinity and various morphologies in an autoclave over a wide temperature range (100–200 °C).[50] Surface oxygen groups and defects on the surface of conductive substrates favor MOF's nucleation and conformal growth, which facilitates the uniform deposition and solid bonding of MOFs on conductive substrates. Yang et al. reported self-supporting Co/Zn-based ZIF (ZIF = zeolitic imidazolate framework) nanosheets on Ni foam (NF) through a facile hydrothermal method (Fig. 3a).[51] In the subsequent heat treatment, linker defects were introduced to increase the intrinsic activity of metal sites and electrical conductivity while maintaining structural integrity. Starting with Ni-BDC (BDC = 1,4-benzenedicarboxylate) on NF synthesized via a hydrothermal method, Sun et al. prepared self-supporting NiRu$_{0.13}$-BDC by introducing atomically dispersed Ru.[52] These two studies related to defect engineering have established an effective

method for regulating the electronic structure of MOFs at the atomic level.

Compared with hydro/solvothermal synthesis, chemical bath deposition is a simpler strategy for fabricating self-supporting MOFs, which occurs under milder conditions (low temperatures and ambient atmosphere).[53] Duan et al. fabricated self-supporting ultrathin two-dimensional (2D) NiFe-MOF/NF nanosheets with high flexibility and rich porosity by a one-step chemical bath deposition strategy (Fig. 3b).[54] This work proposed a universal strategy for self-supporting ultrathin MOFs, which is also applicable to other metal-based 2D MOFs, such as titanium, cobalt, molybdenum, and manganese. Shi et al. reported a self-supporting 2D Ni-CAT (CAT = catecholate) nanowire grown on carbon nanofibers (CNFs).[55] Due to its hierarchical porous structure and core–shell morphology, the self-supporting Ni-CAT nanowire/CNFs provided an efficient transfer pathway for fast electron/ion transport and achieved high-performance actuation behavior. Furthermore, through a general self-dissociation-assembly strategy, Huang et al. synthesized self-supporting well-defined ultrathin CoNi-MOF nanosheets using CoNi alloy foam as substrates and metal ion sources.[56] This work proposed a strategy for preparing self-supporting bimetallic MOFs with highly controllable morphology, providing a new way to prepare excellent non-noble metal electrocatalysts.
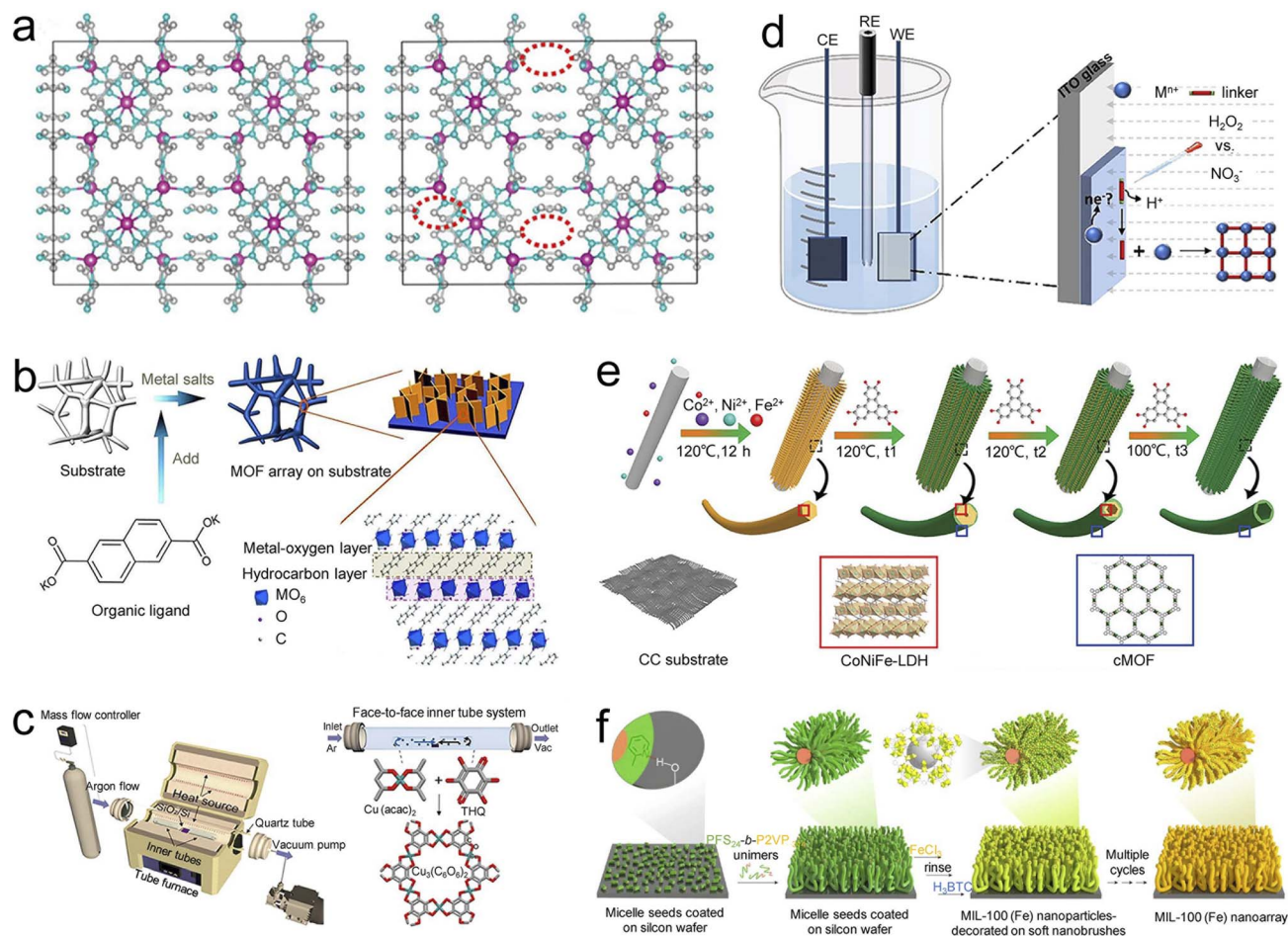
13092 | J. Mater. Chem. A, 2023, **11**, 13089–13106

This journal is © The Royal Society of Chemistry 2023

Fig. 3 Synthesis strategies of self-supporting MOFs. (a) Structure illustration of the ZIFs (left) and ZIFs with linker-deficient (right) prepared by the hydrothermal method. Reproduced with permission from ref. 51. Copyright 2021, WILEY-VCH. (b) Schematic illustration of the chemical bath deposition procedures for ultrathin NiFe-MOF nanosheets. Reproduced with permission from ref. 54. Copyright 2017, Nature Publishing Group. (c) The overall (left) and detailed (right) face-to-face inner tube system setup of chemical vapor deposition for $Cu_3(C_6O_6)_2$. Reproduced with permission from ref. 58. Copyright 2022, American Chemical Society. (d) Schematic illustration of the synthesis procedures of a Cu-BTC film by H_2O_2-assisted cathodic electrodeposition. Reproduced with permission from ref. 60. Copyright 2021, Wiley-VCH. (e) Illustration of the synthetic process of hierarchical porous MOF/LDH heteronanotubes by the template-assisted strategy. Reproduced with permission from ref. 61. Copyright 2021, Wiley-VCH (f) Schematic diagram for the synthesis of MIL-100 (Fe) nanoarrays by the soft nanobrush-directed strategy. Reproduced with permission from ref. 63. Copyright 2022, Nature Publishing Group.

It is worth noting that MOF films have achieved irreplaceable status in practical applications due to their rich topological structure, abundant catalytic active sites, and rapid charge transfer.[57] Chemical vapor deposition (CVD) is a common strategy for preparing low-dimensional materials and MOF films. However, the vapor–solid serial reaction or homopolymerization restricts the application of CVD. Based on this, Choe *et al.* reported a conductive 2D $Cu_3(C_6O_6)_2$ thin film on a SiO_2/Si substrate by all-vapor-phase CVD in a face-to-face inner tube setup (Fig. 3c).[58] The strategy breaks the limitations of the traditional CVD technology and enriches the types of conductive MOF thin films. Furthermore, it is worth mentioning the merits of the electrochemical method, such as mild conditions (normal temperature and pressure), high reaction efficiency, controllable synthesis, environmental protection, and even the most promising to realize the industrial production of MOFs. Most typically, electrodeposition,

which uses a three-electrode/two-electrode electrochemical cell (in which a conductive substrate serves as the working electrode), is a novel method for preparing MOF films.[59] Compared with anode electrodeposition, which relies heavily on the dissolution of the substrate to provide metal ions, cathode deposition is more widely used. Xie *et al.* proposed a hydrogen peroxide-assisted cathode deposition strategy to trigger the deprotonation of MOF ligands at ultra-high potentials (Fig. 3d).[60] This strategy proposes a universal strategy for preparing high-purity MOF thin films, such as Cu-BTC (BTC = benzene-1,3,5-tricarboxylate), Fe-BDC, and Zn-BDC films, which effectively avoids the problem of impurity co-deposition in cathode deposition. Based on the above studies, these strategies related to ultrathin engineering endow MOFs with large specific surface areas and unique quantum properties, showing promise in designing high-performance electrocatalysts.

This journal is © The Royal Society of Chemistry 2023

J. Mater. Chem. A, 2023, **11**, 13089–13106 | **13093**

2.1.2 Template-assisted strategies. Considering the differences in the inherent physical properties of MOFs and the limited nucleation sites on substrates, some MOFs still cannot be directly grown on substrates. In this case, template-assisted strategies (including hard templates and soft templates) offer the possibility of preparing a variety of self-supporting MOFs.

In the hard template-assisted synthesis process, these templates typically undergo three forms of transformation, including complete transformation, partial transformation, and non-conversion; the former often results in a hollow structure and the latter two mostly produce a core–shell structure. For example, by reasonably regulating the synthesis reaction time, Wang et al. demonstrated the process of trimetallic CoNiFe layered double hydroxide (LDH) nanowires as internal templates from partial conversion to complete conversion (Fig. 3e).[61] Conductive MOF (cMOF) nanotubes with a hollow structure were obtained through the complete transformation of the template, while cMOF/LDH heteronanotube arrays with a core–shell structure were obtained through the partial transformation of the template. In a different case, using Ni_3S_2 nanosheets as templates, Wu et al. obtained a Ni_3S_2/MIL-53(Fe) (MIL = Material from Institut Lavoisier) hybrid array grown on NF, in which an MIL-53(Fe) layer was assembled on the surface of Ni_3S_2 nanosheets.[62] Benefiting from ingenious coupling, the obtained self-supporting Ni_3S_2/MIL-53(Fe) composites integrate the advantages of MIL-53(Fe) and Ni_3S_2 and showed excellent OER properties in alkaline solutions.

Except for those mentioned above, a novel way to construct self-supporting MOFs with high aspect ratios and controllable heights is the soft nanobrush-oriented synthesis strategy. Soft nanobrushes are constructed via surface-initiated living crystallization-driven self-assembly. They can capture abundant metal cations through coordination interactions for rapid heterogeneous growth of self-supporting MOFs on various substrates. The synthesis process is divided into two steps: (1) Introducing soft nanobrushes into various substrates through self-assembly driven by surface active living crystals. (2) Synthesizing uniform self-supporting MOFs by alternately immersing the substrate in a metal ion and a ligand solution. Recently, Wang et al. synthesized highly controllable HKUST-1 [$Cu_3(BTC)_2(H_2O)_3$], MIL-100 (Fe), and CUT-8 (Cu) nanoarrays with constant diameter and controllable height within a specific range on various substrates by the soft nanobrush-oriented synthesis strategy (Fig. 3f).[63] The soft nanobrush-oriented synthesis strategy compensates for the harsh reaction conditions of one-step synthesis and breaks through strict restrictions on the composition and shape of hard templates. Besides, it has the advantages of mild experimental conditions, adjustable morphology, and flexible pore size. Notably, it is facile to finely construct hybrid structures with cooperative properties by incorporating additional functional components into self-supporting MOFs. However, the soft nanobrush-oriented synthesis strategy is still restricted to the synthesis of a limited category of MOFs. It is thus necessary to deeply understand the mechanisms of soft nanobrush self-assembly and induction of MOF growth, thereby developing more ligand- or metal-extensible MOFs.

2.1.3 Others. In addition to the above common synthetic strategies, some innovative synthesis methods, such as 3D printing,[64] film forming technology (e.g., microcontact printing, filtration, and liquid-phase epitaxy pump strategy),[65–67] and Langmuir–Blodgett techniques,[68] are also developed for self-supporting MOFs. These strategies will expand the gene pool of self-supporting MOFs and have significant potential for industrial production. In addition, it should be noted that the actual synthesis of self-supporting MOFs often involves the combination of multiple methods, especially in the template-assisted strategy.[69–71] Exploring innovative and general methods and designing rational preparation routes makes it possible to obtain electrocatalysts with desired structures and compositions.

2.2 Derivative strategies of self-supporting MOFs

According to specific conversion methods, MOF precursors can be converted into numerous classes of derivatives (carbon, metal-based compounds, and their composites), inheriting the advantages of MOF precursors and obtaining the desired composition, morphology, and structure. In addition, considering the advantages of self-supporting materials mentioned above, the rational derivative strategies of self-supporting MOFs are also crucial for carrying out a variety of electrochemical reactions. Thus, this section focuses on the latest progress in self-supporting MOF derivative strategies.

2.2.1 Thermal annealing. The thermal annealing strategy is convenient and practical for preparing MOF derivatives with porous structures. Different pyrolysis temperatures and reaction atmospheres usually mean different self-supporting MOF derivatives. Generally speaking, metal oxides are obtained at low temperatures and in an air/oxygen atmosphere; metal carbides can be prepared by self-pyrolysis at high temperatures in an inert atmosphere, while metal sulfides and metal phosphates require additional raw materials to provide sulfur and phosphorus in thermal annealing. In addition, the pyrolysis procedure also significantly impacts the structure of materials. The material may explode when the temperature increases too fast, while when the temperature increases too slowly, the material structure is prone to collapse and damage its integrity.

As a typical example, Zhou et al. fabricated a series of layered structured Co_3O_4@X (X = CoS, CoP, C, and Co_3O_4) composites on a Ni substrate by the sulfurization, phosphorization, carbonization, and oxidation of cobalt carbonate hydroxide@ZIF-67 (Fig. 4a).[72] This work fully demonstrates the impact of reaction conditions on thermal annealing products and is expected to be extended to preparing other composite electrocatalysts with hierarchical structures. Starting with NiCo-MOF microrod arrays, Xu et al. fabricated carbon-confined NiCo@$NiCoO_2$ core@shell nanoparticle arrays by reductive carbonization and subsequently controlled oxidation.[73] The two-step continuous pyrolysis opens a new avenue for designing MOF-derived novel porous bimetallic composite electrocatalysts.

However, traditional pyrolysis strategies usually face problems, such as severe aggregation of metal particles, generation
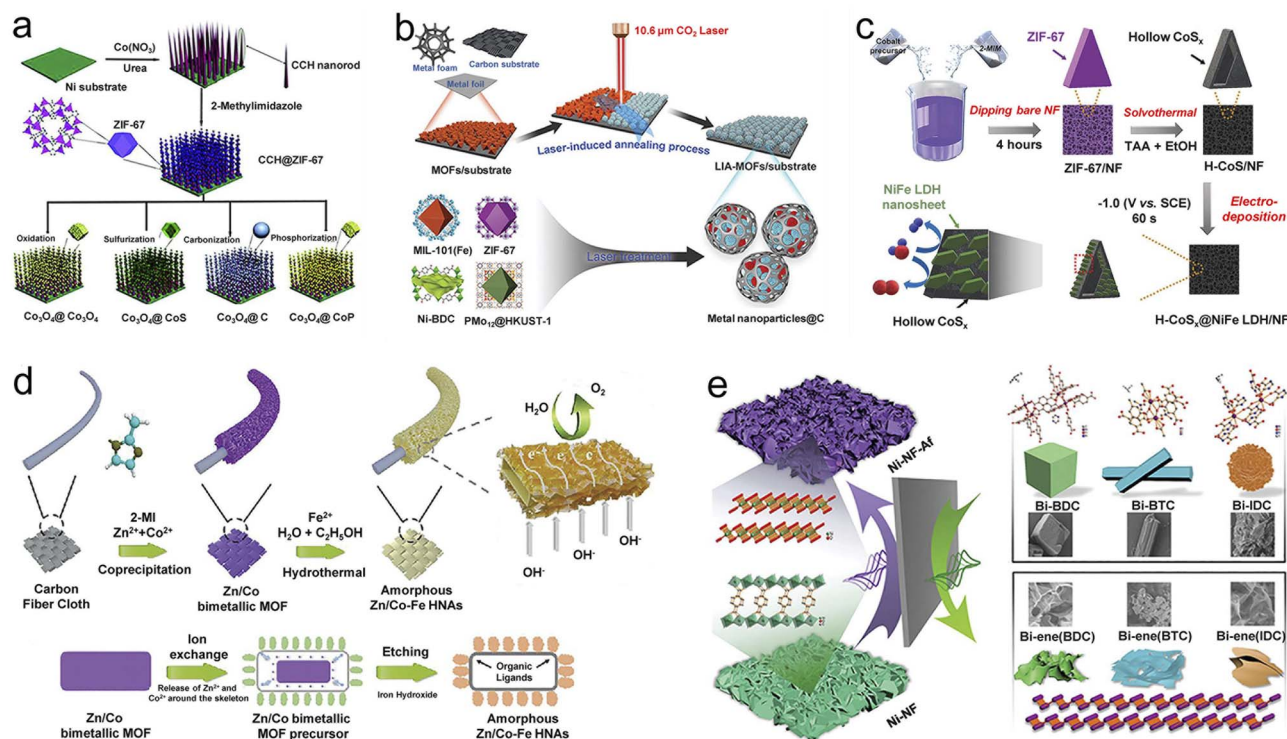
13094 | J. Mater. Chem. A, 2023, **11**, 13089–13106

This journal is © The Royal Society of Chemistry 2023

Fig. 4 Synthesis strategies of self-supporting MOF derivatives. The schematic diagram for the synthesis of (a) hierarchically structured Co_3O_4@X (X = Co_3O_4, CoS, C, and CoP) derived from CCH@ZIF-67 by thermal annealing. Reproduced with permission from ref. 72. Copyright 2017, Wiley-VCH. (b) Various MOFs carbonized by the laser-induced annealing strategy. Reproduced with permission from ref. 74. Copyright 2021, Wiley-VCH. (c) H-CoS$_x$@NiFe LDH/NF derived from ZIF-67 by solvothermal and electrodeposition strategies. Reproduced with permission from ref. 40. Copyright 2022, Wiley-VCH. (d) Zn/Co–Fe HNAs derived from Zn/Co bimetallic-MOF through an ion exchange process. Reproduced with permission from ref. 78. Copyright 2021, Wiley-VCH. (e) Ni-NF-Af derived from Ni-MOFs *via in situ* electrochemical transformation. Reproduced with permission from ref. 80. Copyright 2021, Wiley-VCH.

of harmful gases, and consumption of a lot of time and effort. Tang *et al.* introduced a laser-induced annealing strategy to carbonize MOFs on conductive substrates under ambient conditions to overcome these issues.[74] On account of high local heating temperatures (over 2500 °C) induced by the laser, 12 different MOFs on 8 types of conductive substrates were carbonized rapidly, resulting in core–shell structure derivatives, of which porous carbon shells coated metal nanoparticles (Fig. 4b). The efficient and economic strategy has good potential for the large-scale carbonization of self-supporting MOFs and even other functional materials.

2.2.2 Wet chemical methods. Wet chemical methods involve chemical reactions in the solution phase and are widely used to prepare materials with specific compositions, morphologies, and structures, especially as derivatization strategies for MOFs. Transition metal chalcogenides are typical products obtained by wet chemical methods.[40] For example, Lee *et al.* realized the transformation of ZIF-67 into amorphous hollow CoS$_x$ nanoarrays on NF (Fig. 4c) through the reaction of Co^{2+} released by ZIF-67 reacted with the S^{2-} released by the hydrolysis of acetamide.[75] NiFe LDH was subsequently electrodeposited on the hollow CoS$_x$ surface, and the synthesized hierarchical heterostructured H-CoS$_x$@NiFeLDH/NF exhibited excellent bifunctional catalytic activity for OWS. In addition, Song *et al.* performed a mild hydrothermal vulcanization

treatment on the obtained ZIF-67-Ni(OH)$_2$/NF hybrid, where ZIF-67 was decomposed and gradually released Co^{2+}, and OH^- was replaced by S^{2-} to produce Ni_3S_2.[76] The final product of Co-doped Ni_3S_2 showed good catalytic performance for both the HER and OER under alkaline conditions.

As another typical wet chemical method, the ion exchange method has attracted extensive attention due to its high adjustability toward the structure and morphology of materials.[77] In an interesting report by Gu *et al.*, the H^+ produced by reversible hydrolysis of Fe^{2+} promotes the release of Zn^{2+} and Co^{2+} of Zn/Co-MOF and simultaneously reacts with the hydrolyzed product ferric hydroxide (Fig. 4d).[78] In this ion exchange process, the conversion of bimetallic MOF to amorphous trimetallic Zn/Co–Fe hydroxide-based hollow nanowall arrays on carbon cloth (CC) is achieved. This work presents a simple and energy-saving method for preparing multi-element catalysts with hollow structures and provides valuable ideas for designing high-performance catalysts.

2.2.3 Electrochemical transformation. Electrochemical transformation, another effective strategy to prepare self-supporting MOF derivatives, concerns the removal of organic ligands from pre-synthesized MOFs by cyclic voltammetry (CV) treatment in an alkaline solution.[79] For example, Cao *et al.* used Ni-MOF nanosheet arrays on NF (Ni-NF) as precursors and obtained 2D MOF-derived electrodes (named Ni-NF-Af) by CV

scanning in Ar-saturated 1.0 M KOH (Fig. 4e).[80] When the structure changes from Ni-MOFs to Ni(OH)$_2$, the actual active site Ni^{III} (NiOOH) for the methanol oxidation reaction is generated. Starting with ZIF-L (leaf-like ZIF) on NF, Ding *et al.* obtain amorphous Co(OH)$_2$-ZIF-L/NF by activating the reversible redox of metal ions through a finely controlled electrochemical transformation process.[79] The experimental results and density functional theory (DFT) calculations confirmed that the defective metal oxy(hydroxide) species formed in electrochemical processes are the real active species of the OER. Electrochemical transformation derivative strategies are commonly used to generate metal hydroxide nanoarrays, providing valuable insights into the design of highly active electrocatalysts.

2.2.4 Others. Although there are many derivative strategies, actual cases often involve the systematic and comprehensive application of these methods. For example, Wu *et al.* obtained Mo$_x$–Cu nanocomposites by annealing Cu-based MOF containing a Mo source at 800 °C. They then selectively etched Cu species with a FeCl$_3$ solution to obtain MoC$_x$ octahedra composed of small nanocrystals.[81] Postchemical etching is often used to modify the structure and composition of self-supporting MOF derivatives to remove unwanted components selectively.[82] Moreover, Wang *et al.* converted solid Co-MOF into hollow Ru–Co MOF derivatives by simple Ru^{3+} exchange and ultimately obtained heterogeneous self-supporting (Ru–Co)O$_x$ nanosheets by subsequent pyrolysis.[83] Using Co-MOF as the precursor, Guan *et al.* obtained hollow Ni–Co LDH through ion exchange and etching methods and finally obtained hollow porous NiCo$_2$O$_4$ through pyrolysis at 350 °C in air.[84] These studies demonstrate that desirable chemical compositions and physical properties can be obtained through the deliberate control of the derivatization process, thus providing opportunities for the rational design of flexible and high-performance electrocatalysts.

3. Self-supporting MOF-based hydrogen electrocatalysts

As a clean and sustainable energy carrier, hydrogen is one of the most promising alternatives to traditional fossil fuels in the future. Efficient production and conversion of hydrogen energy are crucial for energy transformation in the future. Therefore, the development of high-performance HER and HOR electrocatalysts has become an attractive research topic in recent years.

3.1 HER

As a cathode reaction of OWS, the HER has received ever-increasing attention in recent years, as its product has the advantages of no pollution, high energy density, and renewability. However, as can be seen from Fig. 1, the HER involves complex multiple proton-coupled reactions, and the slow kinetic reaction often leads to obvious overpotential. Therefore, high-performance electrocatalysts need to be developed to improve energy conversion efficiency. Recently, the

construction of self-supporting MOF-based electrocatalysts has become an effective strategy for solving the above problems.

Pristine MOFs with saturated symmetric coordination metal nodes are not favorable for the Volmer reaction, and their slow water activation kinetics severely hinder HER activity. Therefore, it is essential to regulate metal sites and organic ligands at the atomic level to break the spatial symmetry structure of pristine MOFs. Through ligand regulation strategies, Cheng *et al.* created a unique active region in well-arranged self-supporting Ni-BDC nanosheets with S atoms introduced (Fig. 5a and b).[85] The obtained S-NiBDC with an asymmetric configuration only requires an overpotential of 310 mV to achieve a current density of 10 mA cm^{-2}, along with a Tafel slope of 75 mV dec^{-1} in the alkaline electrolyte (Fig. 5c). Experimental and theoretical studies showed that the improvement of HER performance comes from the acceleration of water activation kinetics by the S-modified Ni site, while the S site in the triangular Ni$_2$–S$_1$ structure acts as the active center for subsequent H$_2$ generation. By carbonizing 2D Co-MOF nanosheets and subsequently phosphating, Hou *et al.* synthesized a 3D superstructure (CoP$_x$@CNS) consisting of well-arranged 2D carbon nanosheets immobilized with ultrafine CoP$_x$ on NF (Fig. 5d and e).[86] CoP$_x$@CNS exhibited excellent HER performance, only requiring an overpotential of 91 mV to achieve 10 mA cm^{-2}, along with a small Tafel slope of 129 mV dec^{-1} in 1.0 M KOH (Fig. 5f and g). The porous 3D superstructure with excellent transport properties of mass/electrons and catalytically active CoP$_x$ nanoparticles with ultrasmall sizes, ultimately boost the HER activities.

Along with those for alkaline conditions, there is a small amount of self-supporting MOF-based HER electrocatalysts under acidic conditions.[87,88] For example, Cai *et al.* reported the synthesis of Pd–CoS$_2$–MoS$_2$/C-600 with excellent HER activity and stability under acidic conditions.[88] Using MoO$_3$@ZIF-6 as a template and precursor, uniform Pd-doped CoS$_2$–MoS$_2$/C was obtained through calcination and the hydrothermal reaction. Benefiting from highly exposed active sites on a unique hollow structure, uniform Pd doping, and fast charge transport, the optimized Pd–CoS$_2$–MoS$_2$/C-600 delivered high catalytic activity with a low overpotential of 144 mV at 10 mA cm^{-2} and a small Tafel slope of 59.9 mV dec^{-1} in 0.5 M H$_2$SO$_4$.

Despite the tremendous excellent HER catalysts that have been developed, there is still a critical bottleneck: most HER catalysts usually operate under acidic or alkaline conditions, which makes it hard to adapt to complex variations of electrolyte concentrations during electrolysis. Thus, developing high-performance HER catalysts over the entire pH range is imperative. For instance, Wang *et al.* reported a 2D/2D heterostructure electrocatalyst composed of an MXene and Co-BDC (Co-BDC/MXene) by a facile ultrasound-assisted strategy (Fig. 5h).[89] Benefiting from the stable 2D/2D heterostructures and Co–O–Ti bond bridging at the interface, Co-BDC/MXene showed superior pH-universal HER activity (Fig. 5i and j). Theoretical studies showed that Co-BDC/MXene heterogeneous catalysts with Co–O–Ti interfacial bridging contribute to optimized Gibbs free energy. This work provides valuable guidance for modulating the electronic configuration of hybrid

13096 | *J. Mater. Chem. A*, 2023, **11**, 13089–13106

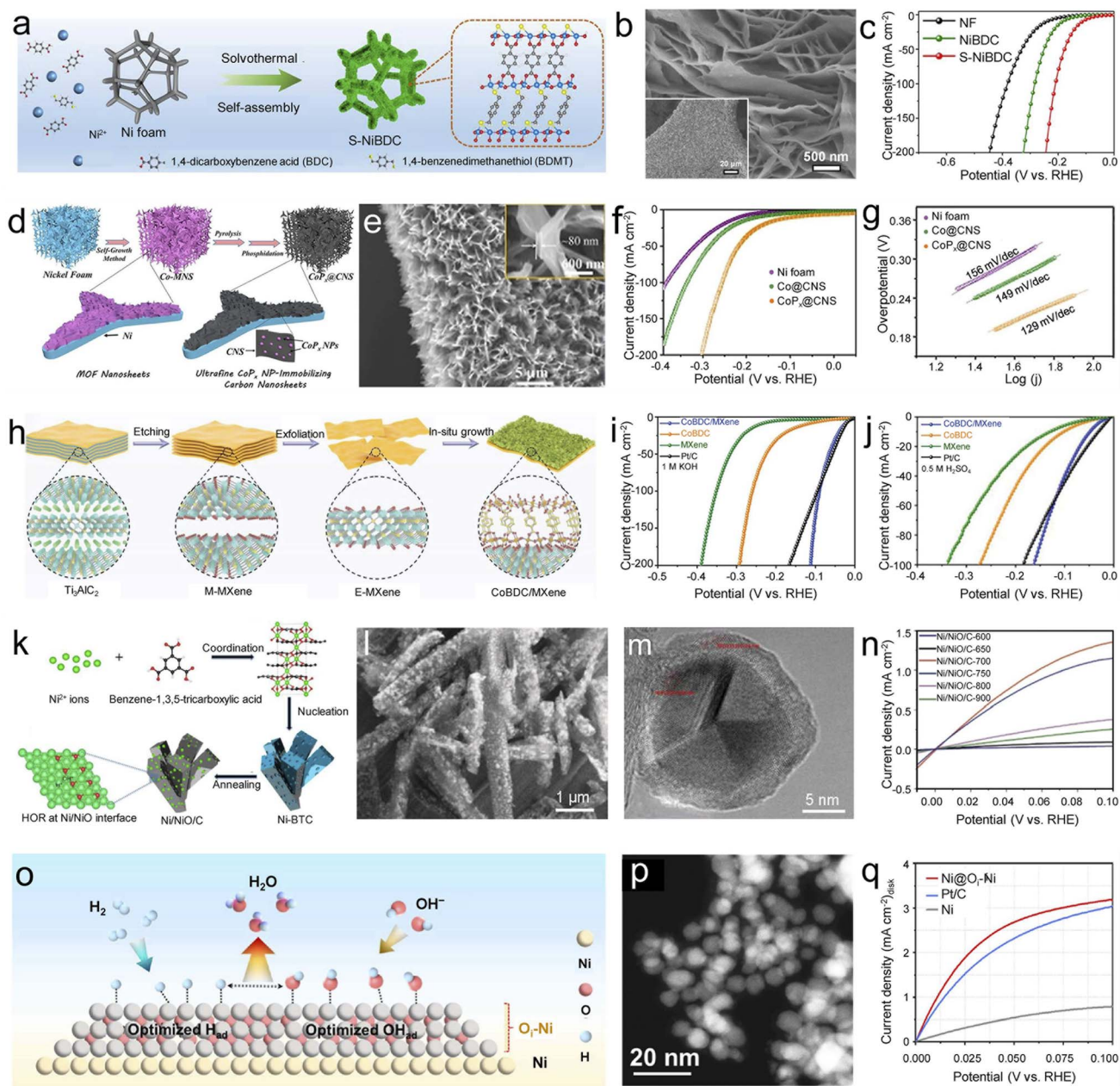This journal is © The Royal Society of Chemistry 2023

Fig. 5   Self-supporting MOF-based electrocatalysts for hydrogen electrocatalysis. (a) Schematic of the synthesis process, (b) scanning electron microscope (SEM) image of S-NiBDC, and (c) polarization curves of different samples for the HER. Reproduced with permission from ref. 85. Copyright 2022, Nature Publishing Group. (d) Schematic diagram, (e) SEM image of CoP_x@CNS, (f) polarization curves, and (g) Tafel slopes of different samples for the HER. Reproduced with permission from ref. 86. Copyright 2020, Wiley-VCH. (h) Schematic diagram of the synthesis of Co-BDC/MXene and the linear sweep voltammetry (LSV) polarization curves of different samples in (i) 1.0 M KOH and (j) 0.5 M H_2SO_4 for the HER. Reproduced with permission from ref. 89. Copyright 2022, Wiley-VCH. (k) Schematic diagram, (l) SEM image, (m) HRTEM image of Ni/NiO/C-700, and (n) polarization curves of Ni/NiO/C-X samples for the HOR. Reproduced with permission from ref. 90. Copyright 2019, Wiley-VCH. (o) The alkaline HOR mechanism, (p) HAADF-STEM image of Ni@O_i-Ni, and (q) polarization curves of different samples for the HOR. Reproduced with permission from ref. 91. Copyright 2022, American Chemical Society.

electrocatalysts, contributing to the rational design of highly active catalytic systems.

3.2   HOR

The efficient utilization of hydrogen energy is an integral part of the hydrogen-based energy system, which is significant in alleviating energy and environmental crises. Low-temperature hydrogen fuel cells, including proton exchange membrane fuel cells (PEMFCs) and anion exchange membrane fuel cells (AEMFCs), are considered the primary way of hydrogen utilization technologies. With the development of platinum-group metal (PGM)-free ORR electrocatalysts with high performance in the alkaline electrolyte, AEMFCs have attracted wide attention because they are more cost-effective and scalable than

This journal is © The Royal Society of Chemistry 2023

J. Mater. Chem. A, 2023, 11, 13089–13106 | 13097

PEMFCs. However, the low kinetics of the HOR process in the alkaline electrolyte makes it a noticeable bottleneck. Therefore, there is an urgent need to find high-performance, low-cost, and earth-abundant HOR electrocatalysts for AEMFCs. Due to their intriguing features of adjustable chemical composition and physical structure, MOFs have also been approved as promising HOR electrocatalysts.

By direct-calcinating Ni-BTC under the protection of graphene layers, Yang et al. synthesized a low-cost Ni/NiO/C catalyst with abundant Ni/NiO interfacial sites, which can be observed clearly in the high-resolution transmission electron microscope (HRTEM) image (Fig. 5k–m).[90] Benefiting from interfaces between NiO and Ni (Fig. 5l and m), the rod-like Ni/NiO/C-700 obtained at 700 °C annealing temperature exhibited higher current density than other samples (Fig. 5n). Experimental and theoretical studies revealed that interfacing Ni and NiO in Ni/NiO/C and the presence of highly conductive graphene layers contribute to optimal binding energies of hydrogen and hydroxide species, ultimately boosting the HOR performance in alkaline electrolytes. Men et al. proposed Ni core nanoparticles coated with oxygen-inserted two atomic-layer Ni shells (Ni@O$_i$-Ni) formed by the low-temperature pyrolysis of Ni-based MOF (Fig. 5o).[91] Uniform distribution of bright Ni nanoparticles can be observed in low magnification high-angle annular dark-field scanning transmission electron microscopy (HAADF-STEM) images (Fig. 5p). The resulting Ni@O$_i$-Ni catalyst showed excellent HOR properties, superior to those of the most advanced Pt/C catalysts (Fig. 5q). Theoretical calculation results showed that the adjustment of the Ni coordination environment contributes to the optimal adsorption/desorption of intermediate species (*OH/*H), which is beneficial to enhance the alkaline HOR performance. By adjusting the atmosphere of pyrolytic Ni$_3$(BTC)$_2$, Ni et al. obtained Ni nanoparticles embedded in N-doped carbon supports (Ni–H$_2$–NH$_3$), showing excellent activity and robustness to the HOR.[92] Based on Ni-based MOF derivatives, these studies optimize the binding energy of hydrogen and hydroxide by regulating the electronic structure, laying the foundation for developing excellent HOR electrocatalysts. However, the research on HOR electrocatalysts is mainly based on PGMs, and the development of MOF-based HOR electrocatalysts is still in the initial stage. Considering the many advantages of MOFs (regular periodic arrangement structure, ligand functionalization, high specific surface area, and accurately controllable pore structure), we boldly predict that MOFs have great potential for the HOR.

4. Self-supporting MOF-based oxygen electrocatalysts

Oxygen electrocatalysts play a significant role in green energy technologies (i.e., OWS, ZABs, and FCs). However, the kinetics of the OER and ORR is extremely slow, which dramatically limits their application in these devices. Therefore, it is necessary to design oxygen electrocatalysts with high performance to improve their efficiency in energy technologies. As an ideal and promising candidate electrocatalyst, the emergence of self-

supporting MOF-based materials provides a feasible solution to the above problems.

4.1 OER

The OER is an integral component of various electrochemical techniques but is hampered by the slow process involving multiple proton-coupled electron transfer processes. Even noble metal-based electrocatalysts, such as IrO$_2$ and RuO$_2$, remain impediments in practical application due to their high price and poor durability. Recently, increasing research efforts have been engaged in constructing self-supporting MOF-based OER electrocatalysts.

For example, using ferrocene dicarboxylic acids as organic ligands, Liang et al. synthesized NiFc-MOF (Fc = ferrocene) on NF by the solvothermal method (Fig. 6a and b).[93] With their unique 2D electronic structure and electron-rich group ferrocene, NiFc-MOF/NF nanosheets exhibited excellent OER properties, with an overpotential of 195 mV at 10 mA cm^{-2} and a low Tafel slope of 48.5 mV dec^{-1} (Fig. 6c). DFT calculations revealed that the Fc units within the MOF crystalline structure enhance the overall electron transfer capacity, which contributes to the enhancement of the OER performance. In addition, by introducing Fc into Co-BDC, self-supporting CoBDC–Fc-NF with a missing linker was obtained by Xue et al. and exhibited excellent activity and robust durability for the OER.[94] These two studies emphasize the importance of regulating the electronic structure in constructing highly efficient self-supporting MOF-electrocatalysts. Starting with two Ni-based MOFs (Ni-BDC-1 and Ni-BDC-3) with different topological and morphologies on NF, Zhang et al. obtained the corresponding products (Ni-BDC-1R and Ni-BDC-3R) by electrochemical CV experiments (Fig. 6d–g).[95] As expected, the MOF heterojunction Ni-BDC-1R with steady and partial reconstruction showed excellent OER performance, significantly better than fully reconstructed Ni-BDC-3R and even comparable to the benchmark IrO$_2$ (Fig. 6h). Theoretical calculation results revealed that the internal electric field formed in the MOF heterojunction optimizes the ad/desorption free energy of the active Ni sites, thus remarkably enhancing the OER performance. This work provides a good model for developing highly efficient OER electrocatalysts through the MOF topology strategy.

Using an in situ coupling strategy, Hong et al. constructed unique heterogeneous composites (Co-ZIF/CDs/CC) by inserting carbon dots (CDs) into self-supporting Co-ZIF nanosheets on CC by a one-pot co-precipitation method.[96] The high coverage of active sites and good conductivity provide the Co-ZIF/CDs/CC an ultralow overpotential of 226 mV at 10 mA cm^{-2}. Benefiting from sophisticated architectures and functional materials, self-supporting MOF composites show great advantages in enhancing electrical conductivity and chemical stability.

Using MOF-74-Co/Fe on NF as precursors, Lu et al. prepared porous NF@PANI@CoFe$_2$O$_4$/C with excellent OER catalytic performance by direct pyrolysis in an N$_2$ atmosphere.[97] Compared with previously complicated processes, this work provided a simple method for preparing metal oxide/carbon

13098 | J. Mater. Chem. A, 2023, **11**, 13089–13106

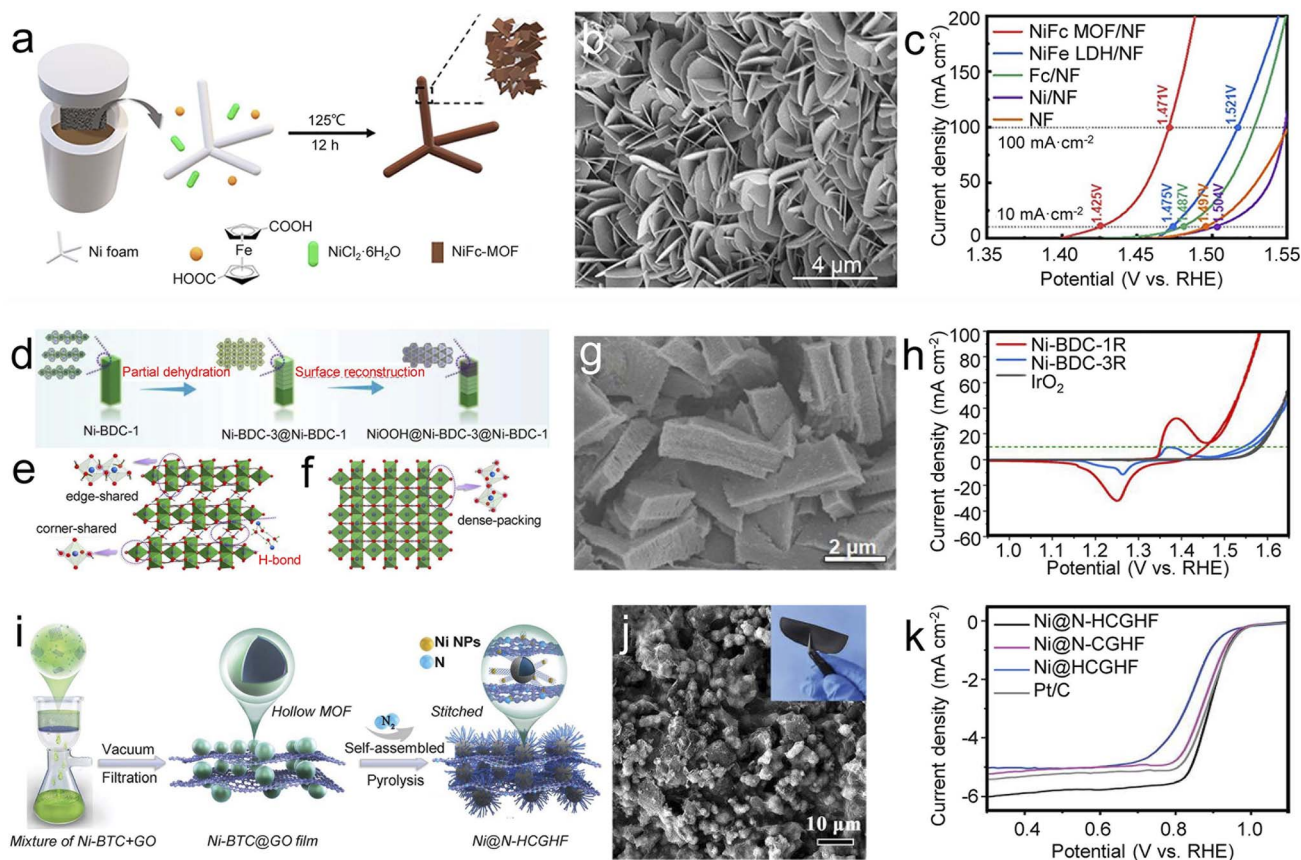This journal is © The Royal Society of Chemistry 2023

Fig. 6 Self-supporting MOF-based electrocatalysts for oxygen electrocatalysis. (a) Illustration of the synthesis, (b) SEM of NiFc-MOF, and (c) LSV curves of different samples for the OER. Reproduced with permission from ref. 93. Copyright 2021, Wiley-VCH. (d) Schematic illustration of the self-reconstruction of an MOF heterojunction and the crystal structures of Ni-BDC-1 (e) and Ni-BDC-3 (f) viewed from an axis, (g) SEM image of Ni-BDC-1R and (h) Tafel plots of different samples for the OER. Reproduced with permission from ref. 95. Copyright 2022, Wiley-VCH. (i) Illustration of the synthesis, (j) top-view SEM image of Ni@N-HCGHF (inset shows a digital image of Ni@N-HCGHF), and (k) LSV curves of different samples for alkaline ORR. Reproduced with permission from ref. 102. Copyright 2020, Wiley-VCH.

composites. In another study on MOF derivations, Li *et al.* converted NiFe-BDC surface-mounted MOFs (SURMOFs) into NiFe-based oxyhydroxide films (SURMOFD) by a simple one-step alkali treatment, in which functional groups such as –Br, –OCH$_3$, and –NH$_2$ were introduced into ligands for stimulating defect strain.[98] Among them, NiFe-BDC (NH$_2$) SURMOFD showed remarkable OER activity and durability. This work highlights the importance of lattice strain in enhancing the activity of self-supporting MOF electrocatalysts.

4.2 ORR

As one of the core processes of renewable energy technology, the cathodic ORR will directly affect the conversion efficiency of FCs and ZABs.[16] The ORR occurs primarily through two different reaction pathways, depending on the nature of the catalysts. In the two-electron pathway, O$_2$ can be converted to H$_2$O$_2$ (acidic medium) and HO$_2^-$ (alkaline medium), which can be further converted to H$_2$O by another subsequent two-electron reaction or to O$_2$ by a chemical disproportionation reaction. In the four-electron pathway, O$_2$ is converted directly to H$_2$O (acidic medium) and OH$^-$ (alkaline medium). When both cost and efficiency are considered in the search for ideal ORR

electrocatalysts, self-supporting MOF-based electrocatalysts stand out for their excellent activity, durability, and methanol resistance among numerous ORR electrocatalysts.

At present, there are only a few reports on MOF-based materials as two-electron ORR electrocatalysts, especially for self-supporting MOF-based materials. Recently, Zhang *et al.* reported ZnCo-ZIFs with an optimized Zn/Co ratio and predominant {001} facets by finely controlling MOFs at the atomic and nano-scale.[99] Experimental results and DFT calculations indicated that the generation of electron insufficient Co active sites and exposure to the {001} surface are favorable for H$_2$O$_2$ desorption and the two-electron ORR. This work opens a new way for the development of advanced MOF-based electrocatalysts for the two-electron ORR.

Compared to the two-electron transfer ORR, the four-electron transfer ORR is more fulfilling for energy technologies. For example, Cheng *et al.* developed a series of lattice strain NiFe MOFs through photoinduced lattice strain.[100] In particular, the current density of 4.3%-MOF (4.3% represents the corresponding lattice expansion ratios) in the potential range 0.5–0.8 V is 5–10 times that of pristine MOFs, even superior to that of commercial Pt/C. This work realizes

controllable electronic structure modulation for self-supporting MOFs *via* lattice strain, which provides a new way to design efficient and low-cost ORR catalysts.

Self-supporting MOF derivatives are more widely used in the ORR than MOFs and their composites, as they are usually endowed with desirable physicochemical properties during the conversion process. Metallic compound/carbon hybrids, a type of MOF derivative in which the derived carbon matrix prevents metallic nanoparticles aggregation and protects them from acid/alkali corrosion. The unique structure and composition facilitate the regulation of the electronic structure and expose abundant active sites, which offers a new paradigm for designing PGM-free electrocatalysts. Co and its compounds with unsaturated electronic structures generally show great potential toward the electrocatalytic ORR. For example, through the carbonization–hydrolysis route, Li *et al.* embedded CeO_2/Co heterostructures in Co-MOF derived N-doped carbon nanosheet arrays (NCNAs) to fabricate self-supporting Co/CeO_2-NCNA@CC for efficient ORR.[101] Theoretical calculation results showed that the Co with unpaired electrons in the Co/CeO_2 heterojunction enhances the oxygen adsorption, thus accelerating the ORR process in the alkaline medium. Apart from self-supporting MOF derived Co-based electrocatalysts, Ni-based materials are another promising ORR electrocatalysts. By pyrolyzing Ni-BTC hollow microspheres/graphene oxide, Wang *et al.* synthesized flexible, freestanding 3D films (Ni@N-HCGHF) stitched from 1D carbon nanotubes and 2D reduced graphene oxide sheets (Fig. 6i and j).[102] Benefitting from the uniform distribution of Ni nanoparticles on an N-doped carbon shell, Ni@N-HCGHF exhibited excellent ORR performance with a half-wave potential of 0.875 V, ranked among the top PGM-free electrocatalysts (Fig. 6k). Experimental and theoretical studies revealed that the N-doped carbon shell coupled with Ni nanoparticles leads to an optimized film with excellent ORR performance.

When the metals in metallic compound/carbon hybrids are controlled from the molecular scale to the atomic scale, another class of MOF derivatives is produced: metal single-atom (SA)-doped carbon materials. Especially transition metal atoms (*i.e.*, Fe, Co, and Ni) coordinated with N-doped carbon materials, typically represented by M–N–C (also known as single-atom catalysts, SACs), usually exhibit excellent ORR activity due to atomically dispersed active sites and highly heterogeneous structures. For example, using ZIFs and electrospun nanofibers as precursors, Ji *et al.* prepared a self-supporting Co SA-anchored N-doped carbon flake on CNFs (Co SA@NCF/CNFs) for highly efficient ORR.[103] Using Co-MOF as a precursor, Zang *et al.* removed Co clusters through the carbonization–acidification process and obtained Co SA anchored in a porous N-doped carbon nanoflake (NC-Co SA). Benefiting from the abundant SA active sites and layered porous structure, the self-supporting SACs derived from MOFs exhibited excellent activity and stability toward the ORR.

5. Energy technologies

Compared with rotating disk electrode (RDE) performance recorded under relatively ideal conditions, membrane electrode

assembly (MEA) performance is much worse due to the difficult mass transfer, insufficient exposure of active sites, low concentration of reaction atmospheres, complex test equipment, and high test temperatures. Therefore, the MEA performance of electrocatalysts must be further improved to realize their practical application. Advanced self-supporting electrocatalysts not only effectively simplify the preparation process and cost of MEAs but also facilitate the integrated construction of the structure and composition of the MEA. With the versatility of MOFs in components, morphology, and structure, self-supporting MOFs are very attractive for constructing high-performance MEAs for energy technologies.

5.1 OWS

Based on the abundance and availability of water resources, OWS contributes to achieving sustainable hydrogen production. Fig. 7a shows the configuration and schematic diagram of a typical OWS. Involving the HER and OER, the actual potential of OWS is usually in the range of 1.8–2.2 V, much higher than the theoretical potential (1.23 V). Although some progress has been made in the development of noble metal-free electrocatalysts for OWS, there is still an urgent need to develop electrocatalysts that can maintain high stability and high activity at high current densities.

For self-supporting pristine MOFs, Zhou *et al.* reported preparing an ultrathin self-supporting defect-Ni-MOF nanosheet array (D-Ni-MOF NSA) with abundant defects by alkali etching (Fig. 7b).[104] The formed unsaturated Ni sites are conducive to exposing more abundant active sites and improving electrical conductivity. When served as both the anode and the cathode for OWS, the D-Ni-MOF NSA only needs a lower and stable voltage of 1.50 V to realize a current density of 10 mA cm^{-2}, which is better than commercial IrO_2/C (+)‖Pt/C (−) (Fig. 7c). Mechanism analysis showed that the formation of open metal sites with high valence states and oxygen vacancies promotes the reduction of rate-determining energy barriers in the OER and HER, while the introduction of K^+ contributes to the rapid charge transfer capability, ultimately boosting the water decomposition activity.

Apart from pristine MOFs, self-supporting MOF composites also show feasibility and prospects for rational construction of OWS device electrodes. Through a controllable grafted-growth strategy, Wang *et al.* obtained a heterogeneous nanotree array catalyst (CoNiRu-NT) by coupling monodisperse Ru metal sites with conductive cMOF/LDH.[105] As expected, the voltage of CoNiRu-NT as a bifunctional OWS electrocatalyst is 1.47 V at a current density of 10 mA cm^{-2}. Research on self-supporting MOF electrocatalysts with monodisperse metal active sites opens up a way for the rational design of bifunctional electrocatalysts.

By electrodepositing NiFe LDH nanosheets onto a hollow CoS_x (H-CoS_x) nanoarray derived from ZIF-67, Lee *et al.* obtained self-supporting H-CoS_x@NiFe LDH/NF.[75] Specifically, the OWS device assembled by using H-CoS_x@NiFe LDH/NF as both the anode and cathode exhibited a cell voltage of 1.98 V to obtain 300 mA cm^{-2}. In addition, Guo *et al.* reported the

13100 | *J. Mater. Chem. A*, 2023, **11**, 13089–13106

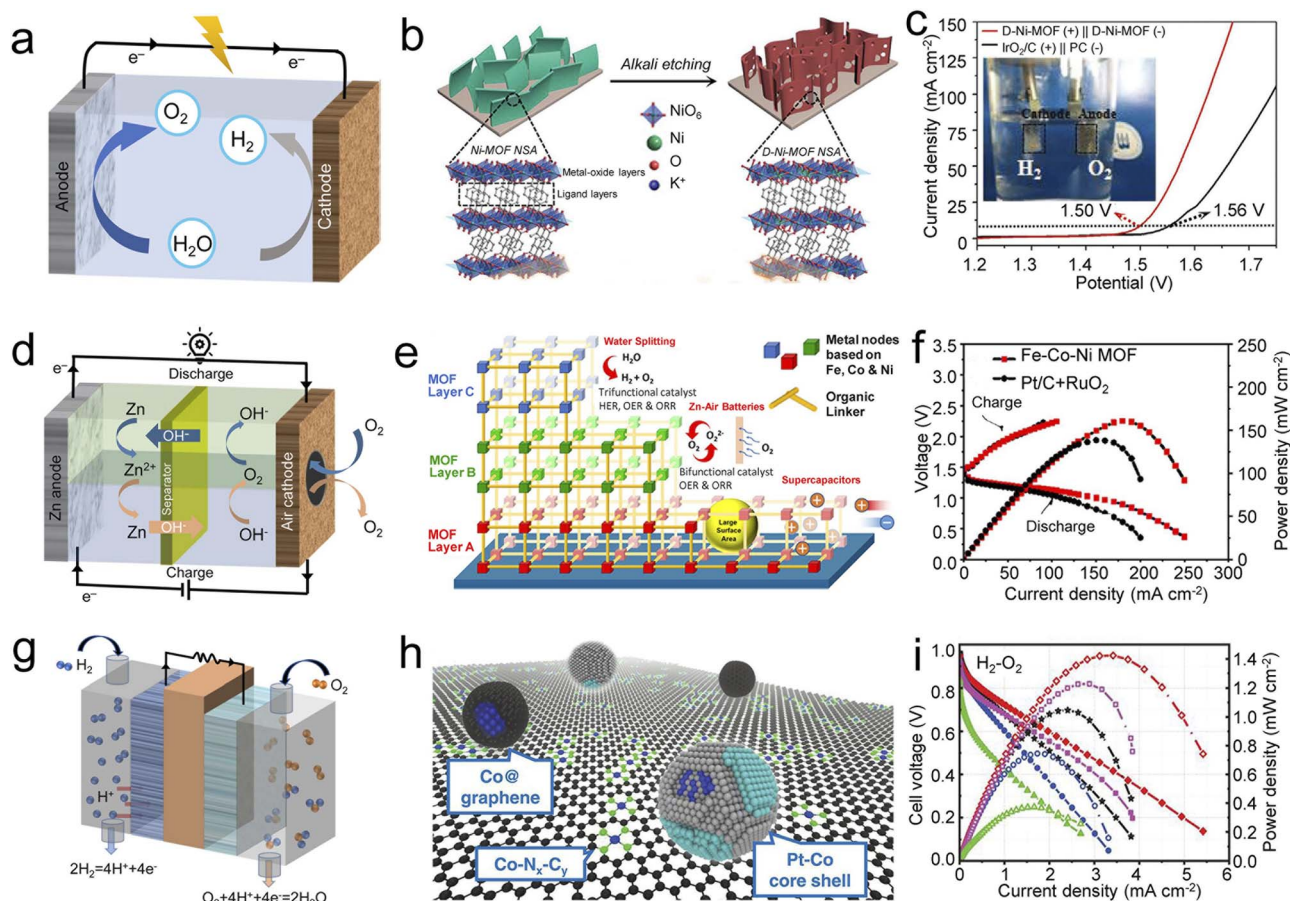This journal is © The Royal Society of Chemistry 2023

Fig. 7 Self-supporting MOF-based electrocatalysts for energy devices. (a) Schematic illustration of OWS devices. (b) Schematic illustration of fabricating a D-Ni-MOF NSA and (c) its LSV plots in water electrolysis. Reproduced with permission from ref. 104. Copyright 2020, Wiley-VCH. (d) Schematic illustration of ZABs. (e) Schematic illustration of trilayer Fe−Co−Ni MOF and (f) its charge−discharge profiles and power density curves of representative Fe−Co−Ni MOF and Pt/C + RuO₂ air-cathodes of ZABs. Reproduced with permission from ref. 109. Copyright 2022, American Chemical Society. (g) Schematic illustration of H₂−O₂ FCs. (h) Schematic diagram of LP@PF catalysts and (i) its current−voltage polarization and power density for H₂−O₂ FCs of LP@PF-1 (black stars), LP@PF-2 (red diamonds), PF-2 (green), 3% Pt₃Co/ZC (blue spheres), and commercial 47% Pt/C (magenta squares). Reproduced with permission from ref. 114. Copyright 2018, American Association for the Advancement of Science.

preparation of Co-NC@Ni₂Fe-LDH by electrodeposition of ultrathin defect-rich Ni₂Fe-LDH nanoarrays onto Co-ZIF-L derived Co-NC microarrays.[106] The electrolyzer based on Co-NC@Ni₂Fe-LDH demonstrates a low cell voltage of 1.55 V at a current density of 10 mA cm⁻² in OWS application. These two studies provide a good model for constructing heterogeneous catalysts derived from self-supporting MOFs.

5.2 ZABs

ZABs have been known as one of the most promising next-generation energy storage systems because of their high energy density, non-polluting emissions, and low cost.[107] Fig. 7d shows the charging and discharging process of ZABs, in which the OER and ORR occur respectively at the air cathode. Given the challenges of slow kinetics and limited mass transfer at air cathodes, the full potential of ZABs has not yet been realized. Considering this, there is an urgent need to develop bifunctional electrocatalysts to effectively solve the issues mentioned above, where self-supporting MOF-based catalysts show tremendous potential.

For example, Jiang et al. obtained Co–Zn heterometallic ZIF (BHZ-48) with hierarchical pores and ligand vacancies by Coᴵᴵ substitution treatment on Zn-based ZIF arrays for 48 h.[108] The ZAB with the BHZ-48 cathode has a discharge–charge voltage gap of 0.8 V and outstanding durability for 760 h at 15 mA cm⁻², which surpasses noble-metal benchmarks. This work provides a new prospect to improve ZABs performance by tuning the ligand environment and heterometallic alliance. By a reduction electrosynthesis method, Farahani prepared layer-by-layer assembled trimetallic Fe–Co–Ni MOF on NF (Fig. 7e).[109] Benefiting from the synergistic effect of Fe, Co, and Ni, rapid mass transfer, and even distribution of abundant active sites, when serving as a bifunctional air cathode electrocatalyst, the Fe–Co–Ni MOF-based ZABs possessed an excellent power density of 161 mW cm⁻² and outstanding specific energy of ∼945 W h kg$_{Zn}^{-1}$, along with long-term stability (Fig. 7f).

Using CoZn-based MOFs grown on a GF (GF = graphene framework) as precursors, Liu et al. obtained a mesoporous CoNC nanocrystal-coated GF by subsequent high-temperature thermal treatment.[69] This work provides insight into the

This journal is © The Royal Society of Chemistry 2023

J. Mater. Chem. A, 2023, 11, 13089–13106 | 13101

reaction mechanism of heteroatom-doped carbon materials in ZABs. In addition, through a facile carbonization–acidification process, Zang et al. fabricated self-supporting Co SA electrocatalysts anchored in porous N-doped carbon flakes derived from Co-MOF precursors.[110] With the high density of Co–N$_x$ active sites, the NC-Co single-atom electrocatalyst demonstrates a high open circuit potential with excellent cycling stabilities when serving as a binder-free air cathode for ZABs.

5.3 FCs

PEMFCs are promising energy conversion systems expected to completely solve the problems of the energy crisis and environmental pollution in the future. In light of different anode fuels, PEMFCs can be divided into H$_2$–O$_2$ FCs, direct ethanol FCs, direct methanol FCs, and direct formic acid FCs.[111] Fig. 7g shows the typical configuration of H$_2$–O$_2$ FC devices. However, their widespread use is severely limited by the slow cathodic ORR process and the scarcity of PGM. As introduced in the ORR section, self-supporting MOF-derived metallic compound/carbon hybrids have attracted much attention due to their excellent ORR performance and have thus also been explored as promising PGM-free electrocatalysts to improve the ORR in H$_2$–O$_2$ FCs.

For example, adopting MOF-5 as the precursor and an Fe(II)–phenanthroline complex as the Fe source, Xie et al. constructed novel Fe SAC-MOF-5 for the ORR in H$_2$–O$_2$ FCs.[112] Compared with other carbon supports, an MOF-5-derived carbon matrix is more accessible to provide abundant active sites, rendering Fe SAC-MOF-5 promising for potential application in H$_2$–O$_2$ FCs. Not limited to single metals, metal alloys/carbon hybrids derived from MOFs also have superior electrocatalytic activity.[113] In a study by Chong et al., PGM-free catalyst substrates PF-1 and PF-2 (PF = PGM-free) were first obtained through thermal activation and controlled acid treatment using ZIF-67 and ZIF-8@ZIF-67 as precursors, respectively. Subsequently, the Pt precursor was introduced into PF-1 and PF-2, and uniformly dispersed PtCo alloys over a substrate of dense Co–N$_x$–C$_y$ sites and onion-like graphitic layers encapsulating Co nanocrystals (named LP@PF-1 and LP@PF-2, respectively) were obtained (Fig. 7h).[114] LP@PF-1 and LP@PF-2 both exhibited excellent catalytic activity and durability in H$_2$–O$_2$ FCs when incorporated in the cathode of the MEA (Fig. 7i). DFT calculations suggested that the interaction between Pt–Co nanoparticles and PGM-free sites improved ORR activity and durability.

In addition to being used as a cathode for FCs, MOFs can also act as a proton exchange membrane (PEM), which is the core component of PEMFCs because of its essential role in transporting protons, separating the reactants, and blocking the direct electron paths within the cells. For example, Zhang et al. mixed MOF-801 and a poly(vinylidene fluoride)–poly(vinylpyrrolidone) matrix (PP-X) to obtain composite membranes, which exhibited high proton conductivity in H$_2$–O$_2$ FCs.[115] Apart from single MOF filled PEMs, dual MOF co-filled hybrid membranes have also been reported. By incorporating acid and basic isomorphic MOFs, namely UiO-66 (SO$_3$H) (abbreviated as A) and UiO-66(NH$_2$) (abbreviated as B) in a chitosan (CS) polymer, Dong et al. reported a low-cost strategy for synthesizing a proton-conducting hybrid membrane (denoted as CS/A + B).[116] CS/A + B possessed excellent proton conductivity
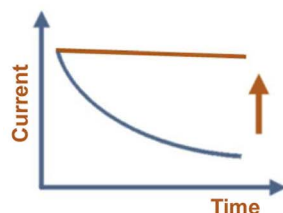

1) Precise Control of Well-defined Structures
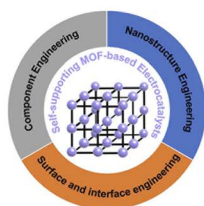
1.1 Component engineering
1.2 Nanostructure engineering
1.3 Surface and interface engineering
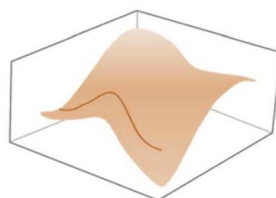
2) Establishment of Measurement and Evaluation Standards

2.1 Unify the experimental test conditions
2.2 Establish performance evaluation standards

3) Long-term Stability

3.1 Modification treatments
3.2 Coating treatments
3.3 Advanced substrates

4) Reaction Mechanism and Structure-Activity Relationship

4.1 In-situ/operando characterizations
4.2 DFT calculations
4.3 Machine learning

5) Practical Applications

5.1 Improve efficiency, selectivity and stability
5.2 Simplify preparation procedures
5.3 Reduce costs

Fig. 8 Proposed future directions of self-supporting MOF-based hydrogen and oxygen electrocatalysts.

13102 | J. Mater. Chem. A, 2023, 11, 13089–13106

This journal is © The Royal Society of Chemistry 2023

at high temperatures benefiting from the synergistic effects between the CS matrix and two isomorphic MOFs. These two studies provide new impetus for the practical application of MOF-based hybrid membranes for PEMs in FCs.

6. Summary and perspectives

In summary, we have thoroughly outlined up-to-date investigations of self-supporting MOF-based hydrogen and oxygen electrocatalysts, with special emphasis on the synthesis strategy and application. Compared with conventional slurry-casting electrodes, self-supporting electrodes skip the requirement of binders and conducting agents, simplify the electrode preparation process, improve mass/charge transport and mechanical stability, and reduce interface resistance. Integrating the superiority of abundant active sites, highly tunable porosity, and large specific surface area, self-supporting MOFs provide an excellent choice for obtaining various advanced hydrogen and oxygen electrocatalysts. However, there is still a long way to go before their practical applications in hydrogen/oxygen-related energy technologies. Herein, several current challenges and potential solutions are described as follows (Fig. 8).

6.1 Precise control of well-defined structures

Firstly, only a handful of the more than 20 000 reported MOFs can be used as self-supporting electrodes, thus rational component engineering is urgently needed to develop more types of self-supporting MOF-based materials for various electrocatalytic reactions. Secondly, MOF derivatives usually undergo severe and irreversible aggregation, shrinkage, fusion, and pulverization during post-processing, thus losing their inherent high specific surface area and porosity. In this case, nanostructure engineering, including the construction of porous, hollow, yolk–shell, frame, hierarchical, and other structures, is an effective strategy to solve these problems. Thirdly, self-supporting MOF-based electrocatalysts are generally unable to exert their advantages due to a lack of effective physicochemical properties. From this point of view, it is essential to adopt surface and interface engineering techniques, such as defect introduction, heterostructure construction, surface functionalization, *etc.*

6.2 Establishment of measurement and evaluation standards

Due to numerous influencing factors, the measurement and evaluation standards of self-supporting MOF-based electrodes have not been unified yet. From the viewpoint of external factors, test conditions, including temperature, pressure, pH, and humidity, obviously influence the activity and stability of self-supporting MOF-based electrodes. For example, the choice of the reference electrode depends significantly on the pH of the electrolyte. Generally, the saturated calomel electrode (SCE) or Hg/Hg_2SO_4 electrode is usually used as the reference electrode in acidic solutions. In neutral solutions, the SCE or Ag/AgCl is recommended as the reference electrode, while Hg/HgO is used in alkaline solutions. From the viewpoint of internal factors, the composition and structure of the catalysts, the choice of substrates, mass load, and binding force also affect the evaluation of self-supporting MOF-based electrodes. For example, the geometric and actual surface areas of many substrates often differ significantly, making it difficult to fairly and objectively compare and evaluate performance parameters related to the surface area. Therefore, unifying experimental test conditions and establishing the corresponding performance evaluation standards is imminent.

6.3 Long-term stability

On the one hand, under the harsh conditions of electrocatalysis (high potential and strong acid/alkaline media), unstable MOFs will undergo structural collapse and even evolve into new phases. On the premise of not blocking active sites and effective mass transfer pore size, further modification and coating treatment can be carried out to improve long-term stability. On the other hand, the choice of advanced substrates is also crucial for the construction of self-supporting MOF-based electrocatalysts. Thus, modifying the substrate surface or developing high-performance conductive substrates is a feasible strategy.

6.4 Reaction mechanism and structure–activity relationship

A thorough understanding of the reaction mechanism is helpful for the rational design of electrocatalysts. Using *in situ*/*operando* characterization techniques to capture reaction intermediates and identify active sites is an indispensable approach to studying the reaction mechanism. It is also the prerequisite for accurately establishing theoretical models in three-phase solutions, thus achieving advanced DFT calculations. In addition, machine learning has also shown strength in analyzing complex chemical processes and modeling materials.

6.5 Practical applications

Considering that the existing synthesis strategies for self-supporting MOF-based electrodes are implemented in the laboratory, it is urgent to achieve industrial scale-up of production technologies. In addition, electrocatalysts face complex working conditions in energy devices, and their efficiency, stability, and selectivity need to be further improved. Therefore, there is an urgent need to develop novel production technologies to meet the demands of practical energy devices.

Author contributions

Xue Feng Lu and Xinchen Wang conceived the original idea and outlined the manuscript structure. Xinran Sun and Xue Feng Lu wrote the original draft and plotted the figures. Sibo Wang, Yidong Hou, Xue Feng Lu, Jiujun Zhang, and Xinchen Wang edited and reviewed the article prior to submission.

Conflicts of interest

There are no conflicts to declare.

This journal is © The Royal Society of Chemistry 2023

J. Mater. Chem. A, 2023, **11**, 13089–13106 | **13103**

Acknowledgements

References

1 R. Xu, L. Du, D. Adekoya, G. Zhang, S. Zhang, S. Sun and Y. Lei, *Adv. Energy Mater.*, 2021, **11**, 2001537.

2 J. Li, X. Jing, Q. Li, S. Li, X. Gao, X. Feng and B. Wang, *Chem. Soc. Rev.*, 2020, **49**, 3565–3604.

3 L. Kong, M. Zhong, W. Shuang, Y. Xu and X.-H. Bu, *Chem. Soc. Rev.*, 2020, **49**, 2378–2407.

4 X. Tang, L. Zhao, W. Sun and Y. Wang, *J. Power Sources*, 2020, **477**, 228919.

5 Z. Liang, T. Qiu, S. Gao, R. Zhong and R. Zou, *Adv. Energy Mater.*, 2021, **12**, 2003410.

6 L. Zu, W. Zhang, L. Qu, L. Liu, W. Li, A. Yu and D. Zhao, *Adv. Energy Mater.*, 2020, **10**, 2002152.

7 B. Zhu, D. Xia and R. Zou, *Coord. Chem. Rev.*, 2018, **376**, 430–448.

8 J. Zhang, G. Chen, K. Mullen and X. Feng, *Adv. Mater.*, 2018, **30**, 1800528.

9 W. Zhang, W. Lai and R. Cao, *Chem. Rev.*, 2017, **117**, 3717–3797.

10 C. Zhang, X. Liang, R. Xu, C. Dai, B. Wu, G. Yu, B. Chen, X. Wang and N. Liu, *Adv. Funct. Mater.*, 2021, **31**, 2008298.

11 L. Liu, Y. Liu and C. Liu, *J. Am. Chem. Soc.*, 2020, **142**, 4985–4989.

12 X. Zhu, X. Tan, K. H. Wu, S. C. Haw, C. W. Pao, B. J. Su, J. Jiang, S. C. Smith, J. M. Chen and R. Amal, *Angew. Chem., Int. Ed.*, 2021, **60**, 21911–21917.

13 Y. Wen, P. Chen, L. Wang, S. Li, Z. Wang, J. Abed, X. Mao, Y. Min, C. T. Dinh and P. D. Luna, *J. Am. Chem. Soc.*, 2021, **143**, 6482–6490.

14 Q. Wang, X. Huang, Z. L. Zhao, M. Wang, B. Xiang, J. Li, Z. Feng, H. Xu and M. Gu, *J. Am. Chem. Soc.*, 2020, **142**, 7425–7433.

15 J. Liu, S. Duan, H. Shi, T. Wang, X. Yang, Y. Huang, G. Wu and Q. Li, *Angew. Chem., Int. Ed.*, 2022, **61**, e202210753.

16 X. Tian, X. F. Lu, B. Y. Xia and X. W. Lou, *Joule*, 2020, **4**, 45–68.

17 X. Long, J. Meng, J. Gu, L. Ling, Q. Li, N. Liu, K. Wang and Z. Li, *Chin. J. Struct. Chem.*, 2022, **41**, 2204046–2204053.

18 W. Li, C. Wang and X. Lu, *Coord. Chem. Rev.*, 2022, **464**, 214555.

19 P. Chen, K. Xu, S. Tao, T. Zhou, Y. Tong, H. Ding, L. Zhang, W. Chu, C. Wu and Y. Xie, *Adv. Mater.*, 2016, **28**, 7527–7532.

20 T. Guo, L. Li and Z. Wang, *Adv. Energy Mater.*, 2022, **12**, 2200827.

21 X. Yan, D. Deng, S. Wu, H. Li and L. Xu, *Chin. J. Struct. Chem.*, 2022, **41**, 2207004–2207015.

22 X. F. Lu, B. Y. Xia, S. Q. Zang and X. W. Lou, *Angew. Chem., Int. Ed.*, 2020, **59**, 4634–4650.

23 Y. Wang, Q. Cao, C. Guan and C. Cheng, *Small*, 2020, **16**, 2002902.

24 B. He, Q. Zhang, Z. Pan, L. Li, C. Li, Y. Ling, Z. Wang, M. Chen, Z. Wang, Y. Yao, Q. Li, L. Sun, J. Wang and L. Wei, *Chem. Rev.*, 2022, **122**, 10087–10125.

25 L. F. Gu, J. J. Chen, T. Zhou, X. F. Lu and G. R. Li, *Nanoscale*, 2020, **12**, 11201–11208.

26 H. Sun, Z. Yan, F. Liu, W. Xu, F. Cheng and J. Chen, *Adv. Mater.*, 2020, **32**, 1806326.

27 H. Yang, M. Driess and P. W. Menezes, *Adv. Energy Mater.*, 2021, **11**, 2102074.

28 C.-F. Li, T.-Y. Shuai, L.-R. Zheng, H.-B. Tang, J.-W. Zhao and G.-R. Li, *Chem. Eng. J.*, 2023, **451**, 138618.

29 J. Liu, S. Liu, F. Yan, Z. Wen, W. Chen, X. Liu, Q. Liu, J. Shang, R. Yu and D. Su, *J. Am. Chem. Soc.*, 2022, **144**, 19106–19114.

30 Q. Zhang, W. Xiao, W. H. Guo, Y. X. Yang, J. L. Lei, H. Q. Luo and N. B. Li, *Adv. Funct. Mater.*, 2021, **31**, 2102117.

31 Q. Wang and D. Astruc, *Chem. Rev.*, 2020, **120**, 1438–1511.

32 Y. Yang, Y. Yang, Y. Liu, S. Zhao and Z. Tang, *Small Sci.*, 2021, **1**, 2100015.

33 H. Wu, J. Wang, W. Jin and Z. Wu, *Nanoscale*, 2020, **12**, 18497–18522.

34 J. Du, F. Li and L. Sun, *Chem. Soc. Rev.*, 2021, **50**, 2663–2695.

35 D. Zhu, M. Qiao, J. Liu, T. Tao and C. Guo, *J. Mater. Chem. A*, 2020, **8**, 8143–8170.

36 B. Zhang, Y. Zheng, T. Ma, C. Yang, Y. Peng, Z. Zhou, M. Zhou, S. Li, Y. Wang and C. Cheng, *Adv. Mater.*, 2021, **33**, 2006042.

37 Z. Meng, N. Chen, S. Cai, R. Wang, J. Wu and H. Tang, *Mater. Chem. Front.*, 2021, **5**, 2649–2667.

38 X. Wen, Q. Zhang and J. Guan, *Coord. Chem. Rev.*, 2020, **409**, 213214.

39 R. Zhuge, P. Shi and T. Zhang, *Chin. J. Struct. Chem.*, 2022, **41**, 2203062–2203069.

40 F. Li, M. Du, X. Xiao and Q. Xu, *ACS Nano*, 2022, **16**, 19913–19939.

41 Z. X. Cai, Z. L. Wang, J. Kim and Y. Yamauchi, *Adv. Mater.*, 2019, **31**, 1804903.

42 R. P. Paitandi, Y. Wan, W. Aftab, R. Zhong and R. Zou, *Adv. Funct. Mater.*, 2022, **33**, 2203224.

43 S. Daliran, A. R. Oveisi, Y. Peng, A. López-Magano, M. Khajeh, R. Mas-Ballesté, J. Alemán, R. Luque and H. Garcia, *Chem. Soc. Rev.*, 2022, **51**, 7810–7882.

44 S. Roy, Z. Huang, A. Bhunia, A. Castner, A. K. Gupta, X. Zou and S. Ott, *J. Am. Chem. Soc.*, 2019, **141**, 15942–15950.

45 N. Heidary, D. Chartrand, A. Guiet and N. Kornienko, *Chem. Sci.*, 2021, **12**, 7324–7333.

46 J. Li, L. Wang, H. He, Y. Chen, Z. Gao, N. Ma, B. Wang, L. Zheng, R. Li, Y. Wei, J. Xu, Y. Xu, B. Cheng, Z. Yin and D. Ma, *Nano Res.*, 2022, **15**, 4986–4995.

47 G. Wang, D. Huang, M. Cheng, S. Chen, G. Zhang, L. Lei, Y. Chen, L. Du, R. Li and Y. Liu, *Coord. Chem. Rev.*, 2022, **460**, 214467.

48 Z. Wang, J. Shen, J. Liu, X. Xu, Z. Liu, R. Hu, L. Yang, Y. Feng, J. Liu and Z. Shi, *Adv. Mater.*, 2019, **31**, 1902228.

49 R. Hou, M. Miao, Q. Wang, T. Yue, H. Liu, H. S. Park, K. Qi and B. Y. Xia, *Adv. Energy Mater.*, 2020, **10**, 1901892.

50 G. Xu, C. Zhu and G. Gao, *Small*, 2022, **18**, 2203140.

13104 | *J. Mater. Chem. A*, 2023, **11**, 13089–13106

This journal is © The Royal Society of Chemistry 2023

51 F. Yang, J. Xie, X. Liu, G. Wang and X. Lu, *Small*, 2021, **17**, 2007085.

52 Y. Sun, Z. Xue, Q. Liu, Y. Jia, Y. Li, K. Liu, Y. Lin, M. Liu, G. Li and C. Y. Su, *Nat. Commun.*, 2021, **12**, 1369.

53 F. Sadegh, S. Akin, M. Moghadam, V. Mirkhani, M. A. Ruiz-Preciado, Z. Wang, M. M. Tavakoli, M. Graetzel, A. Hagfeldt and W. Tress, *Nano Energy*, 2020, **75**, 105038.

54 J. Duan, S. Chen and C. Zhao, *Nat. Commun.*, 2017, **8**, 15341.

55 Y. X. Shi, Y. Wu, S. Q. Wang, Y. Y. Zhao, T. Li, X. Q. Yang and T. Zhang, *J. Am. Chem. Soc.*, 2021, **143**, 4017–4023.

56 L. Huang, G. Gao, H. Zhang, J. Chen, Y. Fang and S. Dong, *Nano Energy*, 2020, **68**, 104296.

57 Z.-G. Gu and J. Zhang, *Coord. Chem. Rev.*, 2019, **378**, 513–532.

58 M. Choe, J. Y. Koo, I. Park, H. Ohtsu, J. H. Shim, H. C. Choi and S. S. Park, *J. Am. Chem. Soc.*, 2022, **144**, 16726–16731.

59 X. Zhang, K. Wan, P. Subramanian, M. Xu, J. Luo and J. Fransaer, *J. Mater. Chem. A*, 2020, **8**, 7569–7587.

60 S. Xie, W. Monnens, K. Wan, W. Zhang, W. Guo, M. Xu, I. F. J. Vankelecom, X. Zhang and J. Fransaer, *Angew. Chem., Int. Ed.*, 2021, **60**, 24950–24957.

61 Y. Wang, L. Yan, K. Dastafkan, C. Zhao, X. Zhao, Y. Xue, J. Huo, S. Li and Q. Zhai, *Adv. Mater.*, 2021, **33**, 2006351.

62 F. Wu, X. Guo, Q. Wang, S. Lu, J. Wang, Y. Hu, G. Hao, Q. Li, M.-Q. Yang and W. Jiang, *J. Mater. Chem. A*, 2020, **8**, 14574–14582.

63 S. Wang, W. Xie, P. Wu, G. Lin, Y. Cui, J. Tao, G. Zeng, Y. Deng and H. Qiu, *Nat. Commun.*, 2022, **13**, 6673.

64 Z. Lyu, G. J. H. Lim, R. Guo, Z. Pan, X. Zhang, H. Zhang, Z. He, S. Adams, W. Chen, J. Ding and J. Wang, *Energy Storage Mater.*, 2020, **24**, 336–342.

65 J.-L. Zhuang, D. Ceglarek, S. Pethuraj and A. Terfort, *Adv. Funct. Mater.*, 2011, **21**, 1442–1447.

66 Y. Mao, G. Li, Y. Guo, Z. Li, C. Liang, X. Peng and Z. Lin, *Nat. Commun.*, 2017, **8**, 14628.

67 D.-J. Li, Q.-H. Li, Z.-G. Gu and J. Zhang, *J. Mater. Chem. A*, 2019, **7**, 18519–18528.

68 G. Xu, T. Yamada, K. Otsubo, S. Sakaida and H. Kitagawa, *J. Am. Chem. Soc.*, 2012, **134**, 16524–16527.

69 S. Liu, M. Wang, X. Sun, N. Xu, J. Liu, Y. Wang, T. Qian and C. Yan, *Adv. Mater.*, 2018, **30**, 1704898.

70 J. Chen, P. Zhuang, Y. Ge, H. Chu, L. Yao, Y. Cao, Z. Wang, M. O. L. Chee, P. Dong, J. Shen, M. Ye and P. M. Ajayan, *Adv. Funct. Mater.*, 2019, **29**, 1903875.

71 J. Gong, W. Luo, Y. Zhao, J. Wang, S. Wang, C. Hu, J. Yang and Y. Dai, *Small*, 2022, **18**, 2204346.

72 J. Zhou, Y. Dou, A. Zhou, R.-M. Guo, M.-J. Zhao and J.-R. Li, *Adv. Energy Mater.*, 2017, **7**, 1602643.

73 H. Xu, Z. X. Shi, Y. X. Tong and G. R. Li, *Adv. Mater.*, 2018, **30**, 1705442.

74 Y. J. Tang, H. Zheng, Y. Wang, W. Zhang and K. Zhou, *Adv. Funct. Mater.*, 2021, **31**, 2102648.

75 Y. J. Lee and S. K. Park, *Small*, 2022, **18**, 2200586.

76 S. Song, Y. Wang, W. Li, P. Tian, S. Zhou, H. Gao, X. Tian and J. Zang, *J. Alloys Compd.*, 2020, **827**, 154299.

77 H. Tan, Y. Zhou, S.-Z. Qiao and H. J. Fan, *Mater. Today*, 2021, **48**, 270–284.

78 Z. Gu, X. Wei, X. Zhang, Z. Duan, Z. Gu, Q. Gong and K. Luo, *Small*, 2021, **17**, 2104125.

79 J. Ding, T. Fan, K. Shen and Y. Li, *Appl. Catal., B*, 2021, **292**, 120174.

80 C. Cao, D. D. Ma, J. Jia, Q. Xu, X. T. Wu and Q. L. Zhu, *Adv. Mater.*, 2021, **33**, 2008631.

81 H. B. Wu, B. Y. Xia, L. Yu, X. Y. Yu and X. W. Lou, *Nat. Commun.*, 2015, **6**, 6512.

82 B. Y. Guan, X. Y. Yu, H. B. Wu and X. W. Lou, *Adv. Mater.*, 2017, **29**, 1703614.

83 C. Wang and L. Qi, *Angew. Chem., Int. Ed.*, 2020, **59**, 17219–17224.

84 C. Guan, X. Liu, W. Ren, X. Li, C. Cheng and J. Wang, *Adv. Energy Mater.*, 2017, **7**, 1602391.

85 F. Cheng, X. Peng, L. Hu, B. Yang, Z. Li, C. L. Dong, J. L. Chen, L. C. Hsu, L. Lei, Q. Zheng, M. Qiu, L. Dai and Y. Hou, *Nat. Commun.*, 2022, **13**, 6486.

86 C. C. Hou, L. Zou, Y. Wang and Q. Xu, *Angew. Chem., Int. Ed.*, 2020, **59**, 21360–21366.

87 K. Karuppasamy, V. R. Jothi, D. Vikraman, K. Prasanna, T. Maiyalagan, B.-I. Sang, S.-C. Yi and H.-S. Kim, *Appl. Surf. Sci.*, 2019, **478**, 916–923.

88 Z. X. Cai, J. Na, J. Lin, A. A. Alshehri, K. A. Alzahrani, Y. G. Alghamdi, H. Lim, J. Zheng, W. Xia, Z. L. Wang and Y. Yamauchi, *Chem.–Eur. J.*, 2020, **26**, 6195–6204.

89 L. Wang, L. Song, Z. Yang, Y. M. Chang, F. Hu, L. Li, L. Li, H. Y. Chen and S. Peng, *Adv. Funct. Mater.*, 2022, **33**, 2210322.

90 Y. Yang, X. Sun, G. Han, X. Liu, X. Zhang, Y. Sun, M. Zhang, Z. Cao and Y. Sun, *Angew. Chem., Int. Ed.*, 2019, **58**, 10644–10649.

91 Y. Men, X. Su, P. Li, Y. Tan, C. Ge, S. Jia, L. Li, J. Wang, G. Cheng, L. Zhuang, S. Chen and W. Luo, *J. Am. Chem. Soc.*, 2022, **144**, 12661–12672.

92 W. Ni, T. Wang, F. Heroguel, A. Krammer, S. Lee, L. Yao, A. Schuler, J. S. Luterbacher, Y. Yan and X. Hu, *Nat. Mater.*, 2022, **21**, 804–810.

93 J. Liang, X. Gao, B. Guo, Y. Ding, J. Yan, Z. Guo, E. C. M. Tse and J. Liu, *Angew. Chem., Int. Ed.*, 2021, **60**, 12770–12774.

94 Z. Xue, K. Liu, Q. Liu, Y. Li, M. Li, C. Y. Su, N. Ogiwara, H. Kobayashi, H. Kitagawa, M. Liu and G. Li, *Nat. Commun.*, 2019, **10**, 5048.

95 L. Zhang, J. Wang, K. Jiang, Z. Xiao, Y. Gao, S. Lin and B. Chen, *Angew. Chem., Int. Ed.*, 2022, **61**, e202214794.

96 Q. Hong, Y. Wang, R. Wang, Z. Chen, H. Yang, K. Yu, Y. Liu, H. Huang, Z. Kang and P. W. Menezes, *Small*, 2023, DOI: **10.1002/smll.202206723**.

97 X. F. Lu, L. F. Gu, J. W. Wang, J. X. Wu, P. Q. Liao and G. R. Li, *Adv. Mater.*, 2017, **29**, 1604437.

98 W. Li, S. Xue, S. Watzele, S. Hou, J. Fichtner, A. L. Semrau, L. Zhou, A. Welle, A. S. Bandarenka and R. A. Fischer, *Angew. Chem., Int. Ed.*, 2020, **59**, 5837–5843.

99 C. Zhang, L. Yuan, C. Liu, Z. Li, Y. Zou, X. Zhang, Y. Zhang, Z. Zhang, G. Wei and C. Yu, *J. Am. Chem. Soc.*, 2023, **145**, 7791–7799.

100 W. Cheng, X. Zhao, H. Su, F. Tang, W. Che, H. Zhang and Q. Liu, *Nat. Energy*, 2019, **4**, 115–122.

This journal is © The Royal Society of Chemistry 2023

J. Mater. Chem. A, 2023, **11**, 13089–13106 | **13105**

101 S. Li, H. Zhang, L. Wu, H. Zhao, L. Li, C. Sun and B. An, *J. Mater. Chem. A*, 2022, **10**, 9858–9868.

102 L. Yan, Y. Xu, P. Chen, S. Zhang, H. Jiang, L. Yang, Y. Wang, L. Zhang, J. Shen, X. Zhao and L. Wang, *Adv. Mater.*, 2020, **32**, 2003313.

103 D. Ji, L. Fan, L. Li, S. Peng, D. Yu, J. Song, S. Ramakrishna and S. Guo, *Adv. Mater.*, 2019, **31**, 1808267.

104 J. Zhou, Y. Dou, X. Q. Wu, A. Zhou, L. Shu and J. R. Li, *Small*, 2020, **16**, 1906564.

105 Y. Wang, S. Wang, Z. L. Ma, L. T. Yan, X. B. Zhao, Y. Y. Xue, J. M. Huo, X. Yuan, S. N. Li and Q. G. Zhai, *Adv. Mater.*, 2022, **34**, 2107488.

106 T. Guo, L. Chen, Y. Li and K. Shen, *Small*, 2022, **18**, 2107739.

107 X. F. Lu, S. L. Zhang, E. Shangguan, P. Zhang, S. Gao and X. W. Lou, *Adv. Sci.*, 2020, **7**, 2001178.

108 Y. Jiang, Y. P. Deng, R. Liang, J. Fu, R. Gao, D. Luo, Z. Bai, Y. Hu, A. Yu and Z. Chen, *Nat. Commun.*, 2020, **11**, 5858.

109 F. Shahbazi Farahani, M. S. Rahmanifar, A. Noori, M. F. El-Kady, N. Hassani, M. Neek-Amal, R. B. Kaner and M. F. Mousavi, *J. Am. Chem. Soc.*, 2022, **144**, 3411–3428.

110 W. Zang, A. Sumboja, Y. Ma, H. Zhang, Y. Wu, S. Wu, H. Wu, Z. Liu, C. Guan, J. Wang and S. J. Pennycook, *ACS Catal.*, 2018, **8**, 8961–8969.

111 Y. Ye, L. Gong, S. Xiang, Z. Zhang and B. Chen, *Adv. Mater.*, 2020, **32**, 1907090.

112 X. Xie, L. Shang, X. Xiong, R. Shi and T. Zhang, *Adv. Energy Mater.*, 2021, **12**, 2102688.

113 S. L. Zhang, X. F. Lu, Z. P. Wu, D. Luan and X. W. Lou, *Angew. Chem., Int. Ed.*, 2021, **60**, 19068–19073.

114 L. Chong, J. Wen, K. Joseph, F. G. Sen, J. Zou, J. Greeley, M. Chan, H. Barkholtz, W. Ding and D.-J. Liu, *Science*, 2018, **362**, 1276–1281.

115 J. Zhang, H. J. Bai, Q. Ren, H. B. Luo, X. M. Ren, Z. F. Tian and S. Lu, *ACS Appl. Mater. Interfaces*, 2018, **10**, 28656–28663.

116 X. Y. Dong, J. H. Wang, S. S. Liu, Z. Han, Q. J. Tang, F. F. Li and S. Q. Zang, *ACS Appl. Mater. Interfaces*, 2018, **10**, 38209–38216.